

Open access • Posted Content • DOI:10.1101/2020.12.23.424169

SARS-CoV-2 sensing by RIG-I and MDA5 links epithelial infection to macrophage inflammation — [Source link](#)

Lucy Thorne, Ann-Kathrin Reuschl, Lorena Zuliani-Alvarez, Matthew Whelan ...+3 more authors

Institutions: University College London

Published on: 23 Dec 2020 - bioRxiv (Cold Spring Harbor Laboratory)

Topics: Innate immune system, Inflammation, Cytokine, Macrophage and RIG-I

Related papers:

- SARS-CoV-2 spike protein S1 subunit induces pro-inflammatory responses via Toll-like receptor 4 signaling in murine and human macrophages
- SARS-CoV-2 Spike protein promotes hyper-inflammatory response that can be ameliorated by Spike-antagonistic peptide and FDA-approved ER stress and MAP kinase inhibitors in vitro
- Protective effects of VIP and PACAP in SARS-CoV-2 infection
- Interaction between Macrophages and Epithelial Cells in Innate Immune Responses against Adenoviral Vectors
- Cellular and Molecular Pathways of COVID-19 and Potential Points of Therapeutic Intervention

Share this paper:    

View more about this paper here: <https://typeset.io/papers/sars-cov-2-sensing-by-rig-i-and-md5-links-epithelial-399uqiergi>

1 **SARS-CoV-2 sensing by RIG-I and MDA5 links epithelial infection to macrophage inflammation**

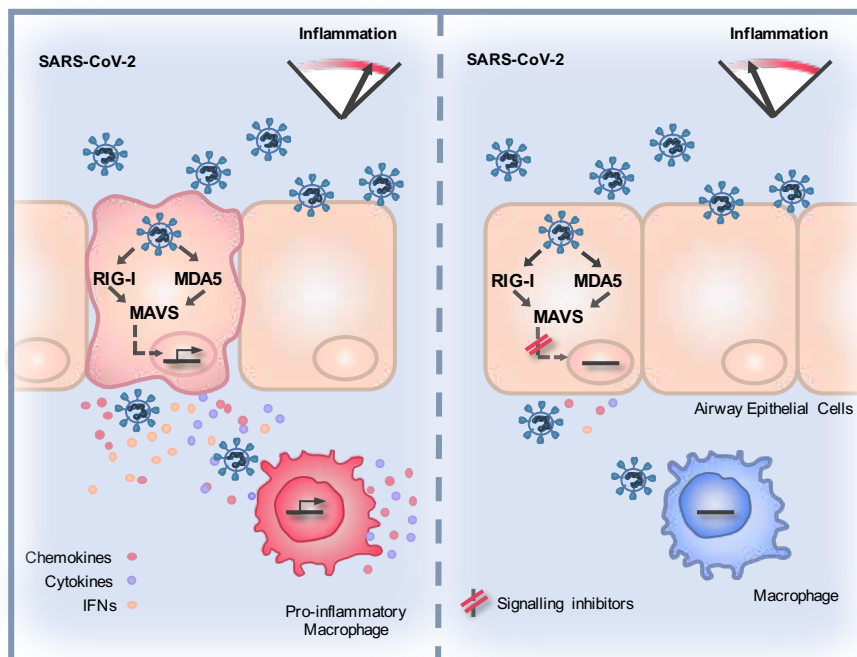
2

3 Lucy G Thorne^{*1+}, Ann-Kathrin Reuschl^{*1}, Lorena Zuliani-Alvarez^{*1}, Matthew V.X. Whelan^{*1}, Mahdad

4 Noursadeghi¹, Clare Jolly^{§1+}, Greg J Towers^{§1+}.

5 ^{*, §}These authors contributed equally. ^{*} Corresponding authors. 1. University College London, Division of
6 Infection and Immunity, University College London, 90 Gower St, London WC1E 6BT, United Kingdom.

7 **Graphical Abstract**



8

9 **Highlights**

- 10 • SARS-CoV-2 activates RNA sensors and consequent inflammatory responses in lung
11 epithelial cells
- 12 • Epithelial RNA sensing responses drive pro-inflammatory macrophage activation
- 13 • Exogenous inflammatory stimuli exacerbate responses to SARS-CoV-2 in both epithelial
14 cells and macrophages
- 15 • Immunomodulators inhibit RNA sensing responses and consequent macrophage
16 inflammation

17 **Summary**

18 SARS-CoV-2 infection causes broad-spectrum immunopathological disease, exacerbated by
19 inflammatory co-morbidities. A better understanding of mechanisms underpinning virus-
20 associated inflammation is required to develop effective therapeutics. Here we discover that
21 SARS-CoV-2 replicates rapidly in lung epithelial cells despite triggering a robust innate immune
22 response through activation of cytoplasmic RNA-sensors RIG-I and MDA5. The inflammatory
23 mediators produced during epithelial cell infection can stimulate primary human macrophages
24 to enhance cytokine production and drive cellular activation. Critically, this can be limited by
25 abrogating RNA sensing, or by inhibiting downstream signalling pathways. SARS-CoV-2 further
26 exacerbates the local inflammatory environment when macrophages or epithelial cells are
27 primed with exogenous inflammatory stimuli. We propose that RNA sensing of SARS-CoV-2 in
28 lung epithelium is a key driver of inflammation, the extent of which is influenced by the
29 inflammatory state of the local environment, and that specific inhibition of innate immune
30 pathways may beneficially mitigate inflammation-associated COVID-19.

31

32 **Introduction**

33 SARS-CoV-2 has caused a devastating pandemic, >74.8 million confirmed cases, >1.6 million
34 deaths (<https://covid19.who.int/>, 20th December 2020) and a worldwide economic crisis.
35 Infection causes a remarkably wide, but poorly understood, disease spectrum, ranging from
36 asymptomatic (Allen et al., 2020;Treibel et al., 2020) to severe acute respiratory distress
37 syndrome, multi-organ failure and death (Docherty et al., 2020;Zhou et al., 2020).

38

39 The success of immunosuppressive corticosteroid dexamethasone in treating COVID-19 (Beigel
40 et al., 2020) suggests the importance of immunopathology in disease, likely driven by immune
41 activation in infected and virus-exposed cells. Intracellular innate immune responses have
42 evolved to detect and suppress invading pathogens, but inappropriate responses can also
43 contribute to disease (Blanco-Melo et al., 2020;Park and Iwasaki, 2020). Pathogen associated
44 molecular patterns (PAMPs) are detected by pattern recognition receptors (PRR), including
45 cytoplasmic nucleic acid sensors, and Toll-like receptors (TLR) that sample extracellular and

46 endosomal space. PRR activation triggers signaling cascades which activate downstream
47 transcription factors, including interferon (IFN) regulatory factors (IRFs) and NF- κ B family
48 members, to initiate a defensive pro-inflammatory gene expression programme, principally
49 mediated by IFN secretion from infected cells. Paracrine and autocrine IFN signalling can suppress
50 viral replication and spread and, together with other secreted cytokines and chemokines,
51 coordinates adaptive immune responses. Viruses have evolved countermeasures to innate
52 defences and deploy a combination of evasion, and direct innate immune pathway antagonism,
53 to promote replication (Sumner et al., 2017). The resulting virus-host conflict is often a significant
54 cause of pathogenesis with PRR-induced inflammation driving disease at the site of replication
55 and systemically (Park and Iwasaki, 2020).

56

57 Missense mutations in innate immune pathways (Pairo-Castineira et al., 2020; Zhang et al., 2020),
58 and autoantibodies leading to deficient Type 1 IFN responses (Bastard et al., 2020), are associated
59 with severe COVID-19 suggesting that intact innate immune responses are important in
60 preventing disease, probably through controlling viral replication. Co-morbidities linked to severe
61 disease are typically inflammatory in nature suggesting that certain types of pre-existing
62 inflammation influence disease severity (Paranjpe et al., 2020). However the specific host-
63 pathogen interactions that cause disease, and how these are impacted by existing inflammation,
64 are not understood. Identification of the molecular events that link viral replication to
65 inflammation and disease will be critical in the development of novel and more precise
66 therapeutic agents. Moreover, such new knowledge will provide insights into the mechanisms by
67 which the associated risk factors for severe COVID-19 impact immune homeostasis in general.

68

69 Here we investigated early host-virus interactions to understand whether SARS-CoV-2 induces an
70 innate response, whether it can escape consequent innate immune control and how it may
71 propagate an immunopathogenic response. We focussed on lung epithelial cells and primary
72 macrophages, which represent cells responsible for the earliest innate immune response to the
73 virus (Bost et al., 2020; Chua et al., 2020). We found rapid replication and infectious virus release
74 in lung epithelial cells prior to potent innate immune activation. Critically, the cocktail of soluble

75 mediators produced by infected cells strongly activated macrophages, which propagated a pro-
76 inflammatory response. RNA sensing of infection by RIG-I and MDA5 was required for inducing
77 the pro-inflammatory milieu as manipulation of the sensing events in epithelial cells, using RNA
78 interference or signalling pathway inhibitors, dampened subsequent macrophage activation and
79 inflammatory gene expression. Pre-exposure of epithelial cells or macrophages to exogenous
80 inflammatory stimuli exacerbated inflammatory responses upon SARS-CoV-2 exposure. We
81 propose that the innate immune microenvironment, in which sensing of SARS-CoV-2 infection
82 occurs, determines the degree of virus-induced inflammation, and has the potential to drive
83 disease.

84

85 **Results**

86 **SARS-CoV-2 activates delayed innate immune responses in lung epithelial cells**

87 In order to investigate innate immune responses to SARS-CoV-2, we first sought a producer cell
88 line that did not respond to the virus, thereby allowing production of virus stocks free of
89 inflammatory cytokines. As adaptive mutations have been reported during passage of the virus
90 in Vero.E6 cells (Davidson et al., 2020;Ogando et al., 2020), we selected human gastrointestinal
91 Caco-2 cells, which express the SARS-CoV-2 receptor ACE2 and entry factors TMPRSS2/4 (Figure
92 S1A, B) and are naturally permissive (Stanifer et al., 2020). We found that Caco-2 support high
93 levels of viral production (Figure S1C, D), but not virus spread (<15% cells infected) (Figure S1E,
94 F). Importantly, they do not mount a detectable innate response to SARS-CoV-2 over 72 hpi at a
95 range of multiplicities of infection (MOIs), as evidenced by a lack of inflammatory gene induction
96 (Figure S1G) and undetectable cytokine secretion. They are also broadly less responsive to innate
97 immune agonists than lung epithelial Calu-3 cells (compare Figure S1H-Caco-2 and S1I-Calu-3).
98 Caco-2 cells were therefore used to produce SARS-CoV-2 stocks uncontaminated by
99 inflammatory cytokines.

100

101 Comparatively, lung epithelial Calu-3 cells express high levels of receptor ACE2, and entry co-
102 factors TMPRSS2 and TMPRSS4 (Figure S1A and B) (Hoffmann et al., 2020;Zang et al., 2020), and

103 are innate immune competent (Figure S1I) when stimulated with various PRR agonists.
104 Consistently, Calu-3 cells supported very rapid spreading infection of SARS-CoV-2 followed by
105 activation of innate immune responses. SARS-CoV-2 replication displayed >1000-fold increase in
106 viral genomic and subgenomic (envelope, E) RNA levels within 5 hours post infection (hpi) across
107 a range of MOIs 0.08, 0.4, 2 TCID50/cell (Figure 1A, Figure S2A), with TCID50 determined in
108 Vero.E6 cells. Genomic and subgenomic E RNA in Calu-3 plateaued around 10 hpi. Rapid
109 spreading infection was evidenced by increasing nucleocapsid protein (N)-positive cells by flow
110 cytometry and immunofluorescence staining, peaking at 24 hpi with 50-60% infected cells
111 (Figures 1B-D and Figure S2B). Infectious virus was evident in supernatants by 5 hpi at the highest
112 MOI and peaked between 10-48 hpi, depending on MOI (Figure 1E, Figure S2C). A pronounced
113 innate immune response to infection followed the peak of viral replication, evidenced by
114 induction of cytokines (IL-6, TNF), chemokines (CCL2, CCL5) and type I and III IFNs (IFN β , IFN λ 1/3)
115 measured by RT-qPCR (Figures 1F and G, and Figure S2D-F). This was accompanied by an IFN-
116 stimulated gene (ISG) expression signature (CXCL10, IFIT1, IFIT2, MxA) (Figure 1H and Figure S2D-
117 F). Gene induction was virus dose-dependent at 24 hpi, but equalised across all MOIs by 48 hpi,
118 as the antiviral response to low-dose virus input maximised. These data show that infected lung
119 epithelial cells can be a direct source of inflammatory mediators.

120
121 We were surprised that SARS-CoV-2 replicated so efficiently in Calu-3 despite innate immune
122 responses including IFN and ISG expression because coronaviruses, including SARS-CoV-2 are
123 reported to be IFN sensitive (Stanifer et al., 2020). Indeed, recombinant Type I IFN, but not type
124 II or type III IFNs, effectively reduced SARS-CoV-2 infection if Calu-3 cells were treated prior to
125 infection (Figure 1I-K, Figure S2G and H). However, Type I IFN had little effect on viral replication
126 when added two hours after infection (Figure 1 I-K). Thus, the IFN response induced in infected
127 lung epithelial Calu-3 cells appears too late to suppress SARS-CoV-2 replication in this system. To
128 determine if viral exposure dose influences the race between viral replication and IFN, we
129 infected cells at a 100x lower dose (MOI 0.0004 TCID50/cell) and observed a longer window of
130 opportunity for exogenous Type I IFN to restrict viral replication (Figure 1 I-K). This is consistent
131 with the hypothesis that high-dose infection can overcome IFN-inducible restriction.

132

133 **Peak SARS-CoV-2 replication precedes innate immune activation**

134 To understand the apparent disconnect in the kinetics between innate immune activation and
135 viral replication, we used single-cell imaging to measure nuclear localisation of activated
136 inflammatory transcription factors NF- κ B p65 and IRF3, which mediate multiple PRR-signalling
137 cascades. NF- κ B p65 nuclear translocation coincided with cells becoming N protein positive and
138 a change was evident from 5 hpi (Figure 2A and B, Figure S3A). The timing of NF- κ B p65
139 translocation was dependant on the viral dose, from 5 hpi for the highest MOI (2 TCID50/cell,
140 Figure S3), between 5 - 10 hpi for MOIs 0.4 and 0.04 (Figures 2A and B, Figure S3), and 24 – 48
141 hpi for MOI 0.004 (Figure S3). IRF3 activation was also virus dose dependent but did not maximise
142 until 72 hpi, later than NF- κ B (Figures 2C and D, Figure S3). These data are consistent with the
143 requirement of a threshold of viral RNA replication to induce transcription factor translocation,
144 particularly for IRF3, and innate immune activation. Although small variation in NF- κ B p65 and
145 IRF3 nuclear intensity was observed in N negative cells, we did not see the same large increases
146 sustained throughout the timecourse as in N positive cells, consistent with direct activation of
147 NF- κ B p65 and IRF3 by virus replication (Figure S3).

148

149 Supporting the observation of activation of NF- κ B p65 and IRF3 activation by SARS-CoV-2
150 infection, single cell fluorescence *in situ* hybridisation (FISH) analysis of IL-6 mRNA (a prototypic
151 NF- κ B regulated cytokine), showed increased IL-6 transcripts uniquely in N-positive infected cells,
152 appearing at 6 hpi and peaking at 24hpi (Figure 2E and F, Figure S4A). IFIT1 transcripts (a
153 prototypic ISG) measured by FISH also demonstrated rapid induction in N-positive cells with
154 increased signal from at 6 hpi (Figure 2H). Strikingly, IFIT1 mRNA was not highly induced in N-
155 negative bystander cells consistent with defective interferon responses failing to induce ISGs and
156 a timely antiviral state in uninfected cells (Figure 2H). As a control for these changes, we show
157 that GAPDH transcripts did not change (Figure S4B). Secretion of pro-inflammatory chemokine
158 CXCL10, and cytokine IL-6, followed gene expression and were detected from 24 hpi (Figure 2I
159 and J, Figure S4C). Further analysis revealed increases in lactate dehydrogenase (LDH) in infected
160 cell supernatants from 48 hpi, equal across all MOIs, indicative of pro-inflammatory cell death

161 (Figure 2K, S4D). Importantly cytokine secretion had also equalised across MOIs from 24 hpi
162 (Figure 2I and J). LDH release paralleled loss of the epithelial monolayer integrity (Figure 1C) and
163 cell death (Figure 2L, Figure S4E and F) accounting for the reduction in cytokine secretion at 72
164 hpi (Figures 2I and J).

165

166 **SARS-CoV-2 is sensed by MDA5 and RIG-I**

167 To determine the mechanism of virus sensing by innate pathways, we first confirmed that viral
168 RNA replication is required for innate immune activation. Inhibition of viral RNA replication, with
169 polymerase inhibitor Remdesivir, abrogated pro-inflammatory and ISG gene expression in a dose-
170 dependent manner (Figure 3A-D). Critically, Remdesivir was only effective if added prior to, or at
171 the time of infection, consistent with a requirement for metabolism to its active tri-
172 phosphorlyated form (Eastman et al., 2020) (Figures 3 E-H).

173

174 Inflammatory gene induction dependent on viral genome replication suggested that an RNA
175 sensor activates this innate response. Both genomic and subgenomic SARS-CoV-2 RNAs are
176 replicated via double stranded intermediates in the cytoplasm (Li et al., 2020). Accordingly, we
177 detected cytoplasmic dsRNA at 5 hpi in Calu-3 cells, preceding N positivity (Figure 3I) and by 48
178 hpi all dsRNA positive cells were N positive. Depletion of RNA sensing adaptor MAVS abolished
179 SARS-CoV-2-induced IL-6, CXCL10, IFN β and IFIT2 gene expression (Figures 3 J-N), consistent with
180 RNA sensing being a key driver of SARS-CoV-2-induced innate immune activation. Concordantly,
181 depletion of cytoplasmic RNA sensors RIG-I or MDA-5 also reduced inflammatory gene expression
182 after infection (Figures 3J-N). This suggested sensing of multiple RNA-species given the different
183 specificities of RIG-I and MDA5 (Hornung et al., 2006; Kato et al., 2006; Rehwinkel et al., 2010; Wu
184 et al., 2013). Intriguingly, unlike RIG-I, MDA5 was not required for induction of IL-6 mRNA,
185 consistent with differences in downstream consequences of RIG-I and MDA5 activation (Figure
186 3M) (Brisse and Ly, 2019). Abrogating SARS-CoV-2 sensing via MDA5 and MAVS depletion also
187 reduced cell death, suggesting cell death is mediated by the host response rather than direct
188 virus-induced damage (Figure 3O). Notably, sensor depletion did not strongly increase viral RNA

189 levels (Figure 3P), or the amount of released infectious virus (Figure 3Q), confirming that innate
190 immune activation via RNA sensing did not potently inhibit viral replication.

191

192 **NF-κB and JAK/STAT signalling drive innate immune responses**

193 As a complementary approach to mapping SARS-CoV-2-induced innate immune activation, and
194 to assess the potential of specific immunomodulators to impact inflammatory responses and viral
195 replication, we examined the effect of inhibiting NF-κB activation using IKK-β kinase (IKK-β)
196 inhibitors TPCA-1 and PS1145. IKK-β is responsible for NF-κB p65 activation by phosphorylation
197 following PRR signalling. Induction of ISGs and IL-6 was inhibited by TPCA-1, and with slightly
198 reduced potency PS1145 (Figure 4A-C, Figure S5A and B). Inhibiting Janus kinase (JAK) with
199 Ruxolitinib, to prevent JAK signalling downstream of the Type I IFN receptor (IFNAR), also
200 suppressed SARS-CoV-2 induced ISGs, but not NF-κB-sensitive IL-6 (Figure 4D-F and Figure S5C).
201 Neither TPCA-1 nor Ruxolitinib treatment increased viral genome replication over a wide range
202 of MOIs (Figure 4G and H) or N positivity or virion production after single dose infection (Figure
203 S5D-F). Importantly, NF-κB and JAK inhibition significantly reduced cell death in infected cultures
204 (Figure 4I). This is consistent with our earlier observation and with the notion that the innate
205 immune response to infection is the main driver of lung epithelial cell damage. Our data thus far,
206 show that SARS-CoV-2 infection of Calu-3 lung epithelial cells results in multi-pathway activation,
207 driving pro-inflammatory and IFN-mediated innate immune responses that are inadequate or
208 arise too late to restrict virus. Critically, they also suggest that SARS-CoV-2 induced IFN and pro-
209 inflammatory gene expression can be therapeutically uncoupled from viral replication.

210

211 **Epithelial responses to SARS-CoV-2 drive macrophage activation**

212 Resident and recruited pro-inflammatory macrophages in the lungs are associated with severe
213 COVID-19 disease (Bost et al., 2020;Liao et al., 2020;Pairo-Castineira et al., 2020;Szabo et al.,
214 2020). We therefore asked whether macrophages can support SARS-CoV-2 infection and how
215 they respond indirectly to infection, through exposure to conditioned medium from infected
216 epithelial cells. Importantly, neither primary monocyte-derived macrophages (MDM), nor PMA-
217 differentiated THP-1 cells (as an alternative macrophage model), supported SARS-CoV-2

replication, evidenced by lack of increase in viral RNA and by the absence of N positive cells (Figures S6A-C). This is consistent with their lack of ACE2 and TMPRSS2 expression (Figure S1A, B). However, exposure of MDM to virus-containing conditioned medium from infected Calu-3 cells (Figure 5A) led to significant macrophage ISG induction (Figure 5B, E, H) and increased expression of macrophage-activation markers CD86 and HLA-DR (Figure 5C-D, F-G, I-J). Importantly, the immune stimulatory activity of conditioned media was dependent on RNA sensing and innate immune activation in infected Calu-3 cells because induction of inflammatory genes and macrophage activation markers was abolished by depletion of MAVS prior to Calu-3 infection (Figure 5B-D) or by inhibition of NF- κ B (TPCA-1) or JAK activation (Ruxolitinib) in infected Calu-3 (Figure 5E-J). Note that in these experiments, MDM were exposed to equivalent numbers of viral genomes from the MAVS depleted, or inhibitor treated conditioned media (Figure S6D-F). These data demonstrate that production of inflammatory mediators from infected lung epithelial cells, downstream of viral RNA sensing, can propagate pro-inflammatory macrophage activation.

232

233 **Pre-existing immune activation exacerbates SARS-CoV-2-dependent inflammation**

234 Severe COVID-19 is associated with inflammatory co-morbidities suggesting that pre-existing
235 inflammatory states lead to inappropriate immune responses to SARS-CoV-2 and drive disease
236 (Lucas et al., 2020; Mehra et al., 2020; Williamson et al., 2020; Wolff et al., 2020; Zhang et al.,
237 2020). Macrophages in particular are thought to potentiate inflammatory responses in the lungs
238 of severe COVID-19 patients (Nicholls et al., 2003; Liao et al., 2020) and so we investigated
239 whether inflammatory stimuli might directly exacerbate macrophage responses to SARS-CoV-2
240 alone (Figure 6A-H). In these experiments we produced virus in Caco-2 and therefore it did not
241 contain inflammatory cytokines (Figure S1G). We detected low level innate immune activation
242 after exposure of MDM to SARS-CoV-2 alone (Figure 6B-H). However, when MDM were primed
243 with 100 ng/ml LPS prior to exposure to SARS-CoV-2, we observed an enhanced response
244 compared to exposure to virus or LPS alone, evidenced by significantly increased levels of ISGs
245 (Figure 6D and E) and pro-inflammatory CCL5 (Figure 6C). Of note, LPS alone induced IL-6 and
246 inflammasome-associated IL-1 β expression and secretion and this was unaffected by virus

247 exposure (Figure 6F-H). Exposure of MDM to SARS-CoV-2, prior to stimulation with LPS (Figure
248 6I-P), also enhanced macrophage inflammatory and ISG responses, but not IL-6 or IL-1 β
249 expression and secretion, compared to those detected with virus or LPS alone (Figure 6J-P). LPS
250 treatment of MDM before or after virus challenge did not induce SARS-CoV-2 permissivity,
251 evidenced by failure to increase the level of detectable viral E gene in MDM supernatants (Figure
252 6B and J).

253

254 Finally, we modelled the lung epithelial cell response to the cytokines observed in activated
255 macrophages. We first selected IL-1 β , as it was produced by LPS-treated, LPS-primed virus-
256 exposed and virus primed LPS-exposed MDM (Figure 6G and H, O and P) and has been observed
257 in severe COVID-19 patient lungs (Laing et al., 2020; Rodrigues et al., 2021). Treatment of Calu-3
258 with IL-1 β during infection significantly increased induction of both ISGs and pro-inflammatory
259 cytokines, compared to their induction by virus alone (Figure 6Q-T). The exception was IL-6,
260 which was highly induced by virus even in the absence of IL-1 β pre-treatment (Figure 6S). Next
261 we treated Calu-3 cells with TNF, which is also produced by LPS-treated or primed MDM (Figure
262 S7A and B) and implicated in severe COVID-19 (Chua et al., 2020; Mahase, 2020), but found no
263 enhancement of innate responses to SARS-CoV-2 (Figure S7C). However, both IL-1 β and TNF
264 treatment increased virus-induced epithelial cell death (Figure 6U and Figure S7D), without
265 impacting viral replication (Figure 6V and Figure S7E). Together, these data suggest that SARS-
266 CoV-2 infection of lung epithelium can promote immune activation of inflammatory
267 macrophages, via secretion of cytokines, chemokines and virus from infected cells, and that this
268 can be exacerbated by a pre-existing pro-inflammatory state. This is consistent with the
269 hypothesis that chronic inflammatory states, rather than enhanced viral replication, drive
270 detrimental immune activation and/or cell death.

271

272

273 **Discussion**

274 We found that SARS-CoV-2 can replicate and spread effectively in lung epithelial Calu-3 cells over
275 a wide range of inoculum doses despite inducing potent IFN responses and ISG expression. We

276 propose that in the model system used here, innate immune activation occurs too late to
277 suppress replication and attribute this to the virus deploying innate immune evasion and
278 antagonism strategies early in infection. Indeed, coronaviruses replicate inside membranous
279 vesicles, thought to protect viral RNA species from cytoplasmic sensing, and have complex
280 capacity to antagonise innate immunity, including inhibition of MDA5 activation (Liu et al., 2020)
281 and preventing nuclear entry of inflammatory transcription factors (Totura and Baric,
282 2012;Banerjee et al., 2020;Miorin et al., 2020;Park and Iwasaki, 2020;Yuen et al., 2020). Indeed,
283 it is possible that the innate immune response and the secreted signals produced by infected
284 cells are dysregulated by viral manipulation, and that this imbalanced response may also
285 contribute to disease when occurring during underlying inflammatory pathology (Blanco-Melo et
286 al., 2020;Giamarellos-Bourboulis et al., 2020;Lucas et al., 2020).

287

288 We demonstrate that SARS-CoV-2 can be sensed by both RIG-I and MDA5 and that, through their
289 signalling adaptor MAVS, these sensors drive inflammatory responses in infected Calu-3 cells.
290 Concordantly, both RIG-I and MDA5 have been implicated in sensing the murine coronavirus
291 mouse hepatitis virus (Roth-Cross et al., 2008;Li et al., 2010) and MDA5 was recently shown to
292 sense SARS-CoV-2 and trigger IFN production (Rebendenne et al., 2020). Likewise, activation of
293 dsRNA sensor PKR has also been observed during SARS-CoV-2 infection of other cell types (Li et
294 al., 2020). The eventual innate immune activation in Calu-3 cells is likely due to sensing of viral
295 RNA when it accumulates to a level that overcomes sequestration and pathway inhibition by the
296 virus, as well as to cellular stress responses to infection. Importantly, Calu-3 cells pre-treated with
297 IFN resist infection illustrating that innate responses can suppress SARS-CoV-2 replication if an
298 antiviral state is induced prior to infection, particularly with a low viral exposure dose.

299

300 Although SARS-CoV-2 RNA has been found associated with macrophages and monocytes from
301 infected patients (Bost et al., 2020), we found that macrophage did not support SARS-CoV-2
302 replication. However, they were sensitive to conditioned media from infected Calu-3 containing
303 virus, IFNs and pro-inflammatory mediators, inducing high levels of chemokine and ISG mRNA
304 and expression of activation markers CD86 and HLA-DR upon exposure. Crucially, it is the

305 response of the Calu-3 cells to virus infection, via RNA sensing, that drives macrophage activation
306 in these experiments, evidenced by suppression of activation after either MAVS depletion or NF-
307 κB (TPCA-1) or JAK inhibition (Ruxolitinib) in the infected Calu-3 cells. Importantly, inhibiting RNA
308 sensing or pathway activation did not particularly increase viral replication, consistent with our
309 observation that, in this model at least, virus-induced innate immune responses do not
310 significantly inhibit SARS-CoV-2 replication. These observations highlight the potential of
311 immunomodulators in reducing SARS-CoV-2 driven inflammatory disease. Indeed, suppression of
312 JAK1/2 signalling with Baricitinib, in SARS-CoV-2 infected macaques, significantly reduced
313 macrophage recruitment and inflammatory signatures and preliminary data support its use in
314 COVID-19 (Bronte et al., 2020). These studies are consistent with epithelial-driven inflammation
315 contributing to myeloid cell infiltration and the role of macrophages in exacerbating immune
316 responses in COVID-19 (Giamparellos-Bourboulis et al., 2020;Hoang et al., 2020;Liao et al., 2020).
317 Our data provide a framework for dissecting immunomodulators as therapeutics and we propose
318 that it is essential to test both immunomodulators, and direct acting antivirals, in innate-immune
319 competent cells, rather than in Caco-2, Vero or other innate immune-inactive cell types, because
320 the inevitable interactions between virus replication and innate immune pathways can influence
321 drug efficacy and potency (Rasaiyah et al., 2013;Kim et al., 2019;Sumner et al., 2020).
322

323 A key question is how our experiments in Calu-3 cells inform understanding of COVID-19. We
324 propose that by studying virus replication in innate immune competent permissive host cells we
325 can probe the earliest interactions between the virus and the host that underpin subsequent
326 inflammatory responses. Our data show that RNA sensing in infected Calu-3 cells creates a pro-
327 inflammatory milieu capable of activating primary macrophages. Crucially the combined profile
328 of pro-inflammatory mediators in this system mirrors that observed in COVID-19 *in vivo* (Bost et
329 al., 2020;Laing et al., 2020;Szabo et al., 2020). We propose that *in vivo* it is the innate immune
330 microenvironment in which the virus-host interaction occurs, and its consequent influence on
331 immune activation, that determines disease outcome. This is consistent with our demonstration
332 that exogenous inflammatory stimuli can drive a state in Calu-3 cells, and primary macrophages,
333 that influences the response to virus, exacerbating inflammation. This link, between the

334 immediate epithelial response to infection and external inflammatory signals, both amplified by
335 macrophages, provides a plausible hypothesis to explain the association of severe COVID-19 with
336 the presence of proinflammatory macrophages in bronchoalvolar lavage and patient lungs
337 (Giamarellos-Bourboulis et al., 2020;Liao et al., 2020;Szabo et al., 2020) and inflammatory co-
338 morbidities (Mehra et al., 2020;Williamson et al., 2020;Wolff et al., 2020), which could provide
339 similar inflammatory stimulation.

340

341 It is remarkable how effective SARS-CoV-2 is in escaping human innate immune responses at the
342 cellular level, despite being a recent zoonosis. Very low levels of adaptive change are consistent
343 with adaptation to human replication prior to identification. Whether SARS-CoV-2 adapted in a
344 non-human species prior to human infection, or whether adaptation in humans occurred before
345 identification, remains unclear. One possibility is that coronaviruses replicate in a conserved
346 niche, with regard to innate immune evasion, and thus are particularly good at zoonosis, perhaps
347 evidenced by SARS-CoV-2 being preceded by SARS-CoV-1 and Middle Eastern Respiratory
348 Syndrome virus (MERS), and apparent cross species transfer and transmission in distantly related
349 species including humans, bats (Boni et al., 2020), camels (Azhar et al., 2014), civet cats (Wang
350 and Eaton, 2007) and mink (Koopmans, 2020).

351

352 Viral disease is often driven by host immune mechanisms that have evolved to protect the host
353 from death, a paradox that is particularly evident in COVID-19. Here we have taken a significant
354 step towards explaining the consequences of SARS-CoV-2 infection of innate immune competent
355 lung epithelial cells by illustrating how RNA sensing can drive potent inflammatory responses,
356 irrespective of whether virus replication is suppressed. We propose that further studies
357 addressing mechanisms of SARS-CoV-2 immune evasion and cytopathology, and the wider impact
358 these have on epithelial-immune cell cross-talk, will inform development of effective
359 therapeutics that are broadly active against zoonotic coronaviruses.

360

361 **Methods**

362 **Cell culture and innate immune stimulation**

363 Calu-3 cells (ATCC HTB-55) and Caco-2 cells were a kind gift Dr Dalan Bailey (Pirbright Institute).
364 THP-1 Dual cells were obtained from Invivogen. Vero.E6 were provided by NIBSC, Beas2B (ATCC
365 CRL-9609) and Hulec5a (ATCC CRL-3244) were obtained from ATCC, and Detroit 562 (ATCC CCL-
366 138) were a kind gift from Dr Caroline Weight (UCL). All cells except THP-1 were cultured in
367 Dulbecco's modified Eagle Medium (DMEM) supplemented with 10% heat-inactivated FBS
368 (Labtech), 100U/ml penicillin/streptomycin, with the addition of 1% Sodium Pyruvate (Gibco) and
369 1% Glutamax for Calu-3 and Caco-2 cells. All cells were passaged at 80% confluence. For
370 infections, adherent cells were trypsinised, washed once in fresh medium and passed through a
371 70 µm cell strainer before seeding at 0.2x10⁶ cells/ml into tissue-culture plates. Calu-3 cells
372 were grown to 60-80% confluence prior to infection. THP-1 cells were cultured in RPMI (Gibco)
373 supplemented with 10 % heat-inactivated FBS (Labtech), 100U/ml penicillin/streptomycin
374 (Gibco), 25 mM HEPES (Sigma), 10 µg/ml of blasticidin (Invivogen) and 100 µg/ml of Zeocin™
375 (Invivogen).Caco-2 and Calu-3 cells were stimulated for 24 h with media containing TLR4 agonist
376 Lipopolysaccharide (LPS) (Peprotech), the TLR3 agonist poly I:C (Peprotech) or the TLR7 agonist
377 R837 (Invivogen), using the concentration stated on each figure. To stimulate RIG-I/MDA5
378 activation in Calu-3 cells, poly I:C was transfected. Transfection mixes were prepared using
379 lipofectamine 2000 (Invitrogen) in Optimem (Thermofisher Scientific) according to the
380 manufacturer's instructions.

381

382 **Isolation of primary monocyte-derived macrophages**

383 Primary monocyte-derived macrophages (MDM) were prepared from fresh blood from healthy
384 volunteers. The study was approved by the joint University College London/University College
385 London Hospitals NHS Trust Human Research Ethics Committee and written informed consent
386 was obtained from all participants. Peripheral blood mononuclear cells (PBMCs) were isolated by
387 density gradient centrifugation using Lymphoprep (Stemcell Technologies). PBMCs were washed
388 three times with PBS and plated to select for adherent cells. Non-adherent cells were washed
389 away after 2 h and the remaining cells incubated in RPMI (Gibco) supplemented with 10 % heat-
390 inactivated pooled human serum (Sigma) and 100 ng/ml macrophage colony stimulating factor
391 (Peprotech). The medium was replaced after 3 days with RPMI with 5% FCS, removing any

392 remaining non-adherent cells. Cells were infected or treated with conditioned media 3-4 days
393 later.

394 **Virus culture and infection**

395 SARS-CoV-2 strain BetaCoV/Australia/VIC01/2020 (NIBSC) was propagated by infecting Caco-2
396 cells at MOI 0.01 TCID50/cell, in DMEM supplemented with 2% FBS at 37°C. Virus was harvested
397 at 72 hours post infection (hpi) and clarified by centrifugation at 4000 rpm for 15 min at 4 °C to
398 remove any cellular debris. Virus stocks were aliquoted and stored at -80 °C. Virus titres were
399 determined by 50% tissue culture infectious dose (TCID50) on Vero.E6 cells. In brief, 96 well
400 plates were seeded at 1x10⁴ cells/well in 100 µl. Eight ten-fold serial dilutions of each virus stock
401 or supernatant were prepared and 50 µl added to 4 replicate wells. Cytopathic effect (CPE) was
402 scored at 5 days post infection, and TCID50/ml was calculated using the Reed & Muench method
403 (Reed, 1938), and an Excel spreadsheet created by Dr. Brett D. Lindenbach was used for
404 calculating TCID50/mL values (Lindenbach, 2009).

405
406 For infections, multiplicities of infection (MOI) were calculated using TCID50/cell determining on
407 Vero.E6 cells. Cells were inoculated with diluted virus stocks for 2h at 37 °C. Cells were
408 subsequently washed twice with PBS and fresh culture medium was added. At indicated time
409 points, cells were harvested for analysis.

410
411 MDM were infected with virus diluted in RPMI, 5% FBS (estimated MOI 0.02 TCID50/cell). MDM
412 were harvested at 24h or 48 hpi for gene expression analysis. For priming experiments, MDM
413 were stimulated with 100 ng/mL of LPS (HC4046, Hycult Biotech) for 2h. Media was replaced and
414 cells were exposed to SARS-CoV-2 as before, diluted in RPMI, 5% FBS. Cells were collected after
415 48h for analysis. Alternatively, cells were mock exposed or exposed to SARS-CoV-2 for 3 days and
416 then stimulated with 100 ng/mL of LPS. Cells were harvested after 24h for analysis.

417
418 **Sensor and adaptor depletion by RNAi**
419 Calu-3 cells were transfected with 40 pmol of siRNA SMART pool against RIG-I (L-012511-00-
420 0005), MDA5 (L-013041-00-0005), MAVS (L-024237-00-0005) or non-targeting control (D-

421 001810-10-05) (Dharmacon) using Lipofectamine *RNAiMAX* Transfection Reagent (Invitrogen).
422 Transfection medium was replaced after 24h with DMEM medium supplemented with 10% FBS,
423 100U/ml penicillin/streptomycin and cells cultured for additional 2 days. On day 3, cells were
424 transfected again with the same siRNA smart pools. Transfection medium was replaced after 24h
425 and cells cultured for additional 2 days before infection. Gene depletion was verified using
426 TaqMan Gene Expression Assay according to manufacturer's instructions detecting human RIG-I
427 (FAM dye-labelled, TaqMan probe ID no. Hs01061436_m1), MAVS (FAM dye-labelled, TaqMan
428 probe ID no. Hs00920075_m1), MDA5 (FAM dye-labelled, TaqMan probe ID no.
429 Hs00223420_m1) or the housekeeping gene OAZ1 (FAM dye-labelled, TaqMan probe ID no.
430 Hs00427923_m1)

431

432 **Treatment with cytokines, inhibitors and conditioned medium**

433 Calu-3 cells were pre-treated with Remdesivir (Selleck Chemicals), TPCA-1 (Biotechne), PS-1145
434 (BioTechne) or Ruxolitinib (Biotechne) at the indicated concentrations or DMSO control at an
435 equivalent dilution for 1 h before SARS-CoV-2 infection unless otherwise stated. Inhibitors were
436 maintained at the indicated concentrations throughout the experiments. For cytokine
437 treatments, recombinant human IFN β , IFN λ 1, IFN λ 2, IFN γ , IL1 β or TNF (Peprotech) at a final
438 concentration of 10 ng/ml were added at the indicated time points. To generate conditioned
439 media (CoM), Calu-3 cells were mock-infected or infected with SARS-CoV-2 at 0.04 TCID50/cell
440 and supernatants were harvested 48 hpi, clarified by centrifugation at 4000 rpm for 15 minutes
441 and 4 °C and stored at -80 °C. For conditioned media experiments, MDM were exposed to CoM
442 as indicated, which was diluted 1:5 in RPMI, 5% FBS. After 6 hours, conditioned medium was
443 replaced with RPMI, 5% FBS and cells were harvested at 48 h for gene expression and surface
444 marker expression analysis.

445 **qRT-PCR**

446 RNA was extracted using RNeasy Micro Kits (Qiagen) and residual genomic DNA was removed
447 from RNA samples by on-column DNase I treatment (Qiagen). Both steps were performed
448 according to the manufacturer's instructions. cDNA was synthesized using SuperScript III with
449 random hexamer primers (Invitrogen). qRT-PCR was performed using Fast SYBR Green Master

450 Mix (Thermo Fisher) for host gene expression or TaqMan Master mix (Thermo Fisher) for viral
 451 RNA quantification, and reactions performed on the QuantStudio 5 Real-Time PCR systems
 452 (Thermo Fisher). Host gene expression was determined using the $2-\Delta\Delta Ct$ method and normalised
 453 to GAPDH expression. Viral RNA copies were deduced by standard curve, using primers and a
 454 Taqman probe specific for E, as described elsewhere (Corman et al., 2020) and below.
 455 The following primers and probes were used:

Target	Sequence
<i>ACE2</i>	Fwd 5'-CGAAGCCGAAGACCTGTTCTA -3' Rev 5'-GGGCAAGTGTGGACTGTTC-3'
<i>CCL5</i>	Fwd: 5'-CCCAGCAGTCGTCTTGTC-3' Rev 5'- TCCCAGAACCCATTCTTCTCT-3'
<i>CXCL10</i>	Fwd 5'-TGGCATTCAAGGAGTACCTC-3' Rev 5'-TTGTAGCAATGATCTAACACG-3'
<i>GAPDH</i>	Fwd 5'-GGGAAACTGTGGCGTGAT-3' Rev 5'-GGAGGAGTGGGTGTCGCTGTT-3'
<i>IFIT1</i>	Fwd 5'-CCTCCTGGGTTCGTCTACA-3' Rev 5'-GGCTGATATCTGGGTGCCTA-3'
<i>IFIT2</i>	Fwd 5'-CAGCTGAGAATTGCACTGCAA-3' Rev 5'-CGTAGGCTGCTCTCCAAGGA-3'
<i>IFNB1</i>	Fwd 5'-AGGACAGGATGAACCTTGAC-3' Rev 5'-TGATAGACATTAGCCAGGAG-3'
<i>IFNL1</i>	Fwd 5'-CACATTGGCAGGTTCAAATCTCT-3' Rev 5'- CCAGCGGACTCCTTTGG-3'
<i>IFNL3</i>	Fwd 5'- TAAGAGGGCCAAAGATGCCCT-3' Rev 5'- CTGGTCCAAGACATCCCC-3'
<i>IL1B</i>	Fwd: 5'- CCTCCTGGGTTCGTCTACA-3' Rev 5'-GGCTGATATCTGGGTGCCTA-3'
<i>IL6</i>	Fwd 5'-AAATTGGTACATCCTCGACG-3' Rev 5'-GGAAGGTTAGGTTGTTTCT-3'
<i>MX1</i>	Fwd 5'-ATCCTGGGATTTGGGGCTT-3' Rev 5'-CCGCTTGTGCGCTGGTGTGCG-3'
<i>TMPRSS2</i>	Fwd 5'-CAAGTGCTCCAACCTCTGGGAT -3' Rev 5'-AACACACCGATTCTCGTCCTC-3'
<i>TMPRSS4</i>	Fwd 5'-ATGCGGAACCTCAAGTGGGC-3' Rev 5'-CTGTTGTGCGTACTGGATGCT-3'
<i>TNF</i>	Fwd 5'-AGCCTCTCTCCTCCTGATCGTG-3' Rev 5'-GGCTGATTAGAGAGAGGTCCCTGG-3'

SARS-CoV-2 E_Sarbeco_F	5'-ACAGGTACGTTAATAGTTAATAGCGT-3'
SARS-CoV-2 E_Sarbeco_Probe1	5'-FAM-ACACTAGCCATCCTACTGCGCTTCG-TAMRA-3'
SARS-CoV-2 E_Sarbeco_R	5'-ATATTGCAGCAGTACGCACACA-3'

456

457 **Cytokine and LDH measurement**

458 Secreted mediators were detected in cell culture supernatants by ELISA. CXCL10 and IL6 protein
 459 were measured using Duoset ELISA reagents (R&D Biosystems) according to the manufacturer's
 460 instructions.

461 Secreted lactate dehydrogenase (LDH) activity was measured as a correlate of cell death in
 462 culture supernatants using Cytotoxicity Detection Kit^{PLUS} (Sigma) according to the manufacturer's
 463 instructions. Culture supernatants were collected at the indicated time points post infection,
 464 clarified by centrifugation and stored at 4 °C until LDH measurement.

465 **Flowcytometry**

466 For flowcytometry analysis, adherent cells were recovered by trypsinising or gentle scraping and
 467 washed in PBS with 2mM EDTA (PBS/EDTA). Non-adherent cells were recovered from culture
 468 supernatants by centrifugation for 5 min at 1600 rpm and washed once in PBS/EDTA. Cells were
 469 stained with fixable Zombie UV Live/Dead dye (Biolegend) for 6 min at room temperature. Excess
 470 stain was quenched with FBS-complemented DMEM. For MDMs, Fc-blocking was performed with
 471 PBS/EDTA+10% human serum for 10 min at 4°C. Cell surface with CD86-Bv711 (IT2.2, Biolegend)
 472 and HLA-DR-PerCpCy5.5 (L243, Biolegend) staining was performed in PBS/EDTA at 4°C for 30min.
 473 Unbound antibody was washed off thoroughly and cells were fixed in 4% PFA prior to intracellular
 474 staining. For intracellular detection of SARS-CoV-2 nucleoprotein, cells were permeabilised for 15
 475 min with Intracellular Staining Perm Wash Buffer (BioLegend). Cells were then incubated with
 476 1µg/ml CR3009 SARS-CoV-2 cross-reactive antibody (a kind gift from Dr. Laura McCoy,) in
 477 permeabilisation buffer for 30 min at room temperature, washed once and incubated with
 478 secondary Alexa Fluor 488-Donkey-anti-Human IgG (Jackson Labs). All samples were acquired on

479 a BD Fortessa X20 or LSR II using BD FACSDiva software. Data was analysed using FlowJo v10 (Tree
480 Star).

481 **Western blotting**

482 For detection of ACE2 expression, whole cell protein lysates were separated by SDS-PAGE,
483 transferred onto nitrocellulose and blocked in PBS with 0.05% Tween 20 and 5% skimmed milk.
484 Membranes were probed with polyclonal goat anti-human ACE2 (1:500, AF933, R&D Biosystems)
485 or rabbit anti-human beat-Actin (1:2500, 6L12, Sigma) followed by donkey anti-goat IRdye
486 680CW or goat anti-rabbit IRdye 800CW (Abcam), respectively. Blots were Imaged using an
487 Odyssey Infrared Imager (LI-COR Biosciences) and analysed with Image Studio Lite software.

488

489 **Immunofluorescence microscopy and RNA-fluorescent *in situ* hybridization**

490 For imaging analysis, Calu-3 or Caco-2 cells were seeded and infected with SARS-CoV-2 in Optical
491 96-well plates (CellCarrier Ultra, PerkinElmer) and cells were fixed with 4% PFA at the indicated
492 timepoints. Permeabilisation was carried out with 0.1% TRITON-X100 (Sigma) in PBS for 15
493 minutes. A blocking step was carried out for 1h at room temperature with 10% goat
494 serum/1%BSA in PBS. Nucleocapsid (N) protein detection was performed by primary incubation
495 with human anti-N antibody (Cr3009, 1ug/ml) for 18h, and washed thoroughly in PBS. Where
496 appropriate, N-protein staining was followed by incubation with rabbit anti-NFkB (p65) (sc-372,
497 Santa Cruz) or rabbit anti-IRF3 (sc-9082, Santa Cruz) for 1 h. Primary antibodies were detected by
498 labelling with with secondary anti-human AlexaFluor488 and anti-rabbit AlexaFluor546
499 conjugates (Jackson Immuno Research) for 1h. For RNA fluorescent *in situ* hybridization (FISH),
500 cells were immunofluorescently labelled for viral N-protein (detected with AlexaFluor488 or
501 AlexaFluor546 conjugates) followed by RNA visualisation using the ViewRNA Cell Plus Kit (Thermo
502 Fisher). The ViewRNA probes implemented targeted *IL-6* (VA4-19075, AlexaFluor488), *IFIT1* (VA4-
503 18833, AlexaFluor488) and *GAPDH* (VA1-10119, AlexaFluor546). All cells were then labelled with
504 HCS CellMask DeepRed (H32721, Thermo Fisher) and Hoechst33342 (H3570, Thermo Fisher).
505 Images were acquired using the WiScan® Hermes High-Content Imaging System (IDEA Bio-
506 medical, Rehovot, Israel) at magnification 10X/0.4NA or 40X/0.75NA. Four channel automated
507 acquisition was carried out sequentially (DAPI/TRITC, GFP/Cy5). For 10X magnification 100%

508 density/100% well area was acquired, resulting in 64 FOV/well. For 40X magnification, 35%
509 density/ 30% well area was acquired resulting in 102 FOV/well.

510

511 **Image analysis**

512 NF- κ B, IRF3, *IL6* and *GAPDH* raw image channels were pre-processed using a batch rolling ball
513 background correction in FIJI imagej software package (Schindelin et al., 2012) prior to
514 quantification. Automated image analysis was carried out using the ‘Athena’ HCS analysis
515 software package (IDEA Bio-medical IDEA Bio-medical, Rehovot, Israel). For quantification of the
516 percentage of nucleocapsid positive cells within the population, the ‘Intracellular Granules’
517 module was utilised. Nuclei were segmented using Hoechst33342 signal. Cell boundaries were
518 determined by segmentation of CellMask signal. Infected cells were determined by thresholding
519 intracellular N protein signal (Intracellular granules). For all analysis, the N protein signal intensity
520 was thresholded against the mock infected wells to ensure no false segmentation of N +ve
521 objects. Nuclear accumulation of NF- κ B or IRF3 was carried out using the ‘Intranuclear Foci’
522 module. Nuclei of cells were segmented using the Hoechst33342 stain. ‘Foci’ of perinuclear N
523 protein signal were identified and an ‘Infected’ cell population determined based on the presence
524 of such segmented foci objects. In all cells the NF- κ B or IRF3 signal present within segmented
525 nuclei was quantified. For RNA-FISH quantification the ‘Mitochondria’ module was implemented.
526 Nuclei were segmented using the Hoechst33342 stain. Cell cytoplasmic area was determined by
527 segmentation of CellMask 647 signal. Intracellular N protein signal was segmented as
528 ‘mitochondria’ objects. *IL-6/GAPDH* RNA FISH signal within segmented cells was then quantified.
529 Infected cells were determined by the presence of N protein segmented objects within the cell.
530 Analysis parameters are detailed in Supplementary Table 1A-C.

531

532 **Statistical analysis**

533 Statistical analysis was performed using GraphPad Prism. As indicated, normally distributed data
534 was analysed for statistical significance by *t*- tests (when comparing two groups) or one-way
535 ANOVA with Bonferroni or Dunnett’s post-test (when comparing more than two groups).
536 Wilcoxon ranked paired non-parametric tests were performed for primary macrophage data that

537 was not normally distributed. For imaging analysis, where appropriate, integrated intensities
538 were normalised to the mean intensity of the mock infected population for that respective
539 timepoint. Comparisons were made using a Kruskal-Wallis test with Dunn's multiple comparison.
540 Data show the mean +/- the S.E.M, where appropriate the median is shown, with significance
541 shown on the figures, levels were defined as *, P < 0.05; **, P < 0.01 and ***, P < 0.001, ****, P
542 < 0.0001.

543

544 **Acknowledgements**

545 MN and CJ were funded by Wellcome Investigator Awards, and GJT was funded by a Wellcome
546 Senior Fellowship. Funds were also obtained from the University College London COVID-19 fund
547 and the National Institutes of Health Research UCL/UCLH Biomedical Research Centre. We are
548 grateful to Giada Mattiuzzo at NIBSC for SARS-CoV-2 and reagents, Laura McCoy at UCL for SARS-
549 CoV-2 N antibody, Dalan Bailey at The Pirbright Institute and Richard Milne at UCL for valuable
550 discussions and critical reading of the manuscript.

551

552 **References**

- 553 Allen, W.E., Altae-Tran, H., Briggs, J., Jin, X., Mcgee, G., Shi, A., Raghavan, R., Kamariza, M.,
554 Nova, N., Pereta, A., Danford, C., Kamel, A., Gothe, P., Milam, E., Aurambault, J., Primke,
555 T., Li, W., Inkenbrandt, J., Huynh, T., Chen, E., Lee, C., Croatto, M., Bentley, H., Lu, W.,
556 Murray, R., Travassos, M., Coull, B.A., Openshaw, J., Greene, C.S., Shalem, O., King, G.,
557 Probasco, R., Cheng, D.R., Silbermann, B., Zhang, F., and Lin, X. (2020). Population-scale
558 longitudinal mapping of COVID-19 symptoms, behaviour and testing. *Nat Hum Behav* 4,
559 972-982.
- 560 Azhar, E.I., El-Kafrawy, S.A., Farraj, S.A., Hassan, A.M., Al-Saeed, M.S., Hashem, A.M., and
561 Madani, T.A. (2014). Evidence for camel-to-human transmission of MERS coronavirus. *N
562 Engl J Med* 370, 2499-2505.
- 563 Banerjee, A.K., Blanco, M.R., Bruce, E.A., Honson, D.D., Chen, L.M., Chow, A., Bhat, P.,
564 Ollikainen, N., Quinodoz, S.A., Loney, C., Thai, J., Miller, Z.D., Lin, A.E., Schmidt, M.M.,
565 Stewart, D.G., Goldfarb, D., De Lorenzo, G., Rihn, S.J., Voorhees, R.M., Botten, J.W.,
566 Majumdar, D., and Guttman, M. (2020). SARS-CoV-2 Disrupts Splicing, Translation, and
567 Protein Trafficking to Suppress Host Defenses. *Cell* 183, 1325-1339.e1321.
- 568 Bastard, P., Rosen, L.B., Zhang, Q., Michailidis, E., Hoffmann, H.H., Zhang, Y., Dorgham, K.,
569 Philippot, Q., Rosain, J., Béziat, V., Manry, J., Shaw, E., Haljasmägi, L., Peterson, P.,
570 Lorenzo, L., Bizien, L., Trouillet-Assant, S., Dobbs, K., De Jesus, A.A., Belot, A., Kallaste,
571 A., Catherinot, E., Tandjaoui-Lambotte, Y., Le Pen, J., Kerner, G., Bigio, B., Seeleuthner,

- 572 Y., Yang, R., Bolze, A., Spaan, A.N., Delmonte, O.M., Abers, M.S., Aiuti, A., Casari, G.,
573 Lampasona, V., Piemonti, L., Ciceri, F., Bilguvar, K., Lifton, R.P., Vasse, M., Smadja, D.M.,
574 Migaud, M., Hadjadj, J., Terrier, B., Duffy, D., Quintana-Murci, L., Van De Beek, D.,
575 Roussel, L., Vinh, D.C., Tangye, S.G., Haerynck, F., Dalmau, D., Martinez-Picado, J.,
576 Brodin, P., Nussenzweig, M.C., Boisson-Dupuis, S., Rodríguez-Gallego, C., Vogt, G.,
577 Mogensen, T.H., Oler, A.J., Gu, J., Burbelo, P.D., Cohen, J.I., Biondi, A., Bettini, L.R.,
578 D'angio, M., Bonfanti, P., Rossignol, P., Mayaux, J., Rieux-Laukat, F., Husebye, E.S., Fusco,
579 F., Ursini, M.V., Imberti, L., Sottini, A., Paghera, S., Quiros-Roldan, E., Rossi, C.,
580 Castagnoli, R., Montagna, D., Licari, A., Marseglia, G.L., Duval, X., Ghosn, J., Tsang, J.S.,
581 Goldbach-Mansky, R., Kisand, K., Lionakis, M.S., Puel, A., Zhang, S.Y., Holland, S.M.,
582 Gorochov, G., Jouanguy, E., Rice, C.M., Cobat, A., Notarangelo, L.D., Abel, L., Su, H.C.,
583 and Casanova, J.L. (2020). Autoantibodies against type I IFNs in patients with life-
584 threatening COVID-19. *Science* 370.
- 585 Beigel, J.H., Tomashek, K.M., Dodd, L.E., Mehta, A.K., Zingman, B.S., Kalil, A.C., Hohmann, E.,
586 Chu, H.Y., Luetkemeyer, A., Kline, S., Lopez De Castilla, D., Finberg, R.W., Dierberg, K.,
587 Tapson, V., Hsieh, L., Patterson, T.F., Paredes, R., Sweeney, D.A., Short, W.R., Touloumi,
588 G., Lye, D.C., Ohmagari, N., Oh, M.-D., Ruiz-Palacios, G.M., Benfield, T., Fätkenheuer, G.,
589 Kortepeter, M.G., Atmar, R.L., Creech, C.B., Lundgren, J., Babiker, A.G., Pett, S., Neaton,
590 J.D., Burgess, T.H., Bonnett, T., Green, M., Makowski, M., Osinusi, A., Nayak, S., and
591 Lane, H.C. (2020). Remdesivir for the Treatment of Covid-19 — Final Report. *New
592 England Journal of Medicine* 383, 1813-1826.
- 593 Blanco-Melo, D., Nilsson-Payant, B.E., Liu, W.C., Uhl, S., Hoagland, D., Möller, R., Jordan, T.X.,
594 Oishi, K., Panis, M., Sachs, D., Wang, T.T., Schwartz, R.E., Lim, J.K., Albrecht, R.A., and
595 Tenoever, B.R. (2020). Imbalanced Host Response to SARS-CoV-2 Drives Development of
596 COVID-19. *Cell* 181, 1036-1045.e1039.
- 597 Boni, M.F., Lemey, P., Jiang, X., Lam, T.T., Perry, B.W., Castoe, T.A., Rambaut, A., and Robertson,
598 D.L. (2020). Evolutionary origins of the SARS-CoV-2 sarbecovirus lineage responsible for
599 the COVID-19 pandemic. *Nat Microbiol* 5, 1408-1417.
- 600 Bost, P., Giladi, A., Liu, Y., Bendjelal, Y., Xu, G., David, E., Blecher-Gonen, R., Cohen, M.,
601 Medaglia, C., Li, H., Deczkowska, A., Zhang, S., Schwikowski, B., Zhang, Z., and Amit, I.
602 (2020). Host-Viral Infection Maps Reveal Signatures of Severe COVID-19 Patients. *Cell*
603 181, 1475-1488.e1412.
- 604 Brisse, M., and Ly, H. (2019). Comparative Structure and Function Analysis of the RIG-I-Like
605 Receptors: RIG-I and MDA5. *Frontiers in Immunology* 10.
- 606 Bronte, V., Ugel, S., Tinazzi, E., Vella, A., De Sanctis, F., Canè, S., Batani, V., Trovato, R., Fiore, A.,
607 Petrova, V., Hofer, F., Barouni, R.M., Musiu, C., Caligola, S., Pinton, L., Torroni, L., Polati,
608 E., Donadello, K., Friso, S., Pizzolo, F., Iezzi, M., Facciotti, F., Pelicci, P.G., Righetti, D.,
609 Bazzoni, P., Rampudda, M., Comel, A., Mosaner, W., Lunardi, C., and Olivieri, O. (2020).
610 Baricitinib restrains the immune dysregulation in patients with severe COVID-19. *J Clin
611 Invest* 130, 6409-6416.
- 612 Chua, R.L., Lukassen, S., Trump, S., Hennig, B.P., Wendisch, D., Pott, F., Debnath, O., Thürmann,
613 L., Kurth, F., Völker, M.T., Kazmierski, J., Timmermann, B., Twardziok, S., Schneider, S.,
614 Machleidt, F., Müller-Redetzky, H., Maier, M., Krannich, A., Schmidt, S., Balzer, F., Liebig,
615 J., Loske, J., Suttorp, N., Eils, J., Ishaque, N., Liebert, U.G., Von Kalle, C., Hocke, A.,

- 616 Witzenrath, M., Goffinet, C., Drosten, C., Laudi, S., Lehmann, I., Conrad, C., Sander, L.E.,
617 and Eils, R. (2020). COVID-19 severity correlates with airway epithelium-immune cell
618 interactions identified by single-cell analysis. *Nat Biotechnol* 38, 970-979.
- 619 Corman, V.M., Landt, O., Kaiser, M., Molenkamp, R., Meijer, A., Chu, D.K., Bleicker, T., Brünink,
620 S., Schneider, J., Schmidt, M.L., Mulders, D.G., Haagmans, B.L., Van Der Veer, B., Van
621 Den Brink, S., Wijsman, L., Goderski, G., Romette, J.-L., Ellis, J., Zambon, M., Peiris, M.,
622 Goossens, H., Reusken, C., Koopmans, M.P., and Drosten, C. (2020). Detection of 2019
623 novel coronavirus (2019-nCoV) by real-time RT-PCR. *Euro surveillance : bulletin
624 Europeen sur les maladies transmissibles = European communicable disease bulletin* 25,
625 2000045.
- 626 Davidson, A.D., Williamson, M.K., Lewis, S., Shoemark, D., Carroll, M.W., Heesom, K.J., Zambon,
627 M., Ellis, J., Lewis, P.A., Hiscox, J.A., and Matthews, D.A. (2020). Characterisation of the
628 transcriptome and proteome of SARS-CoV-2 reveals a cell passage induced in-frame
629 deletion of the furin-like cleavage site from the spike glycoprotein. *Genome Med* 12, 68.
- 630 Docherty, A.B., Harrison, E.M., Green, C.A., Hardwick, H.E., Pius, R., Norman, L., Holden, K.A.,
631 Read, J.M., Dondelinger, F., Carson, G., Merson, L., Lee, J., Plotkin, D., Sigfrid, L., Halpin,
632 S., Jackson, C., Gamble, C., Horby, P.W., Nguyen-Van-Tam, J.S., Ho, A., Russell, C.D.,
633 Dunning, J., Openshaw, P.J., Baillie, J.K., and Semple, M.G. (2020). Features of 20 133 UK
634 patients in hospital with covid-19 using the ISARIC WHO Clinical Characterisation
635 Protocol: prospective observational cohort study. *Bmj* 369, m1985.
- 636 Eastman, R.T., Roth, J.S., Brimacombe, K.R., Simeonov, A., Shen, M., Patnaik, S., and Hall, M.D.
637 (2020). Remdesivir: A Review of Its Discovery and Development Leading to Emergency
638 Use Authorization for Treatment of COVID-19. *ACS Cent Sci* 6, 672-683.
- 639 Giamarellos-Bourboulis, E.J., Netea, M.G., Rovina, N., Akinosoglou, K., Antoniadou, A.,
640 Antonakos, N., Damoraki, G., Gkavogianni, T., Adami, M.E., Katsaounou, P., Ntaganou,
641 M., Kyriakopoulou, M., Dimopoulos, G., Koutsodimitropoulos, I., Velissaris, D.,
642 Koufargyris, P., Karageorgos, A., Katrini, K., Lekakis, V., Lupse, M., Kotsaki, A., Renieris,
643 G., Theodoulou, D., Panou, V., Koukaki, E., Koulouris, N., Gogos, C., and Koutsoukou, A.
644 (2020). Complex Immune Dysregulation in COVID-19 Patients with Severe Respiratory
645 Failure. *Cell Host Microbe* 27, 992-1000.e1003.
- 646 Hoang, T.N., Pino, M., Boddapati, A.K., Viox, E.G., Starke, C.E., Upadhyay, A.A., Gumber, S.,
647 Nekorchuk, M., Busman-Sahay, K., Strongin, Z., Harper, J.L., Tharp, G.K., Pellegrini, K.L.,
648 Kirejczyk, S., Zandi, K., Tao, S., Horton, T.R., Beagle, E.N., Mahar, E.A., Lee, M.Y.H.,
649 Cohen, J., Jean, S.M., Wood, J.S., Connor-Stroud, F., Stammen, R.L., Delmas, O.M.,
650 Wang, S., Cooney, K.A., Sayegh, M.N., Wang, L., Filev, P.D., Weiskopf, D., Silvestri, G.,
651 Waggoner, J., Piantadosi, A., Kasturi, S.P., Al-Shakhshir, H., Ribeiro, S.P., Sekaly, R.P.,
652 Levit, R.D., Estes, J.D., Vanderford, T.H., Schinazi, R.F., Bosinger, S.E., and Paiardini, M.
653 (2020). Baricitinib treatment resolves lower-airway macrophage inflammation and
654 neutrophil recruitment in SARS-CoV-2-infected rhesus macaques. *Cell*.
- 655 Hoffmann, M., Kleine-Weber, H., Schroeder, S., Krüger, N., Herrler, T., Erichsen, S., Schiergens,
656 T.S., Herrler, G., Wu, N.H., Nitsche, A., Müller, M.A., Drosten, C., and Pöhlmann, S.
657 (2020). SARS-CoV-2 Cell Entry Depends on ACE2 and TMPRSS2 and Is Blocked by a
658 Clinically Proven Protease Inhibitor. *Cell* 181, 271-280.e278.

- 659 Hornung, V., Ellegast, J., Kim, S., Brzózka, K., Jung, A., Kato, H., Poeck, H., Akira, S., Conzelmann,
660 K.K., Schlee, M., Endres, S., and Hartmann, G. (2006). 5'-Triphosphate RNA is the ligand
661 for RIG-I. *Science* 314, 994-997.
- 662 Kato, H., Takeuchi, O., Sato, S., Yoneyama, M., Yamamoto, M., Matsui, K., Uematsu, S., Jung, A.,
663 Kawai, T., Ishii, K.J., Yamaguchi, O., Otsu, K., Tsujimura, T., Koh, C.S., Reis E Sousa, C.,
664 Matsuura, Y., Fujita, T., and Akira, S. (2006). Differential roles of MDA5 and RIG-I
665 helicases in the recognition of RNA viruses. *Nature* 441, 101-105.
- 666 Kim, K., Dauphin, A., Komurlu, S., Mccauley, S.M., Yurkovetskiy, L., Carbone, C., Diehl, W.E.,
667 Strambio-De-Castillia, C., Campbell, E.M., and Luban, J. (2019). Cyclophilin A protects
668 HIV-1 from restriction by human TRIM5α. *Nat Microbiol* 4, 2044-2051.
- 669 Koopmans, M. (2020). SARS-CoV-2 and the human-animal interface: outbreaks on mink farms.
670 *Lancet Infect Dis*.
- 671 Laing, A.G., Lorenc, A., Del Molino Del Barrio, I., Das, A., Fish, M., Monin, L., Muñoz-Ruiz, M.,
672 Mckenzie, D.R., Hayday, T.S., Francos-Quijorna, I., Kamdar, S., Joseph, M., Davies, D.,
673 Davis, R., Jennings, A., Zlatareva, I., Vantourout, P., Wu, Y., Sofra, V., Cano, F., Greco, M.,
674 Theodoridis, E., Freedman, J., Gee, S., Chan, J.N.E., Ryan, S., Bugallo-Blanco, E., Peterson,
675 P., Kisand, K., Haljasmägi, L., Chadli, L., Moingeon, P., Martinez, L., Merrick, B.,
676 Bisnauthsing, K., Brooks, K., Ibrahim, M.a.A., Mason, J., Lopez Gomez, F., Babalola, K.,
677 Abdul-Jawad, S., Cason, J., Mant, C., Seow, J., Graham, C., Doores, K.J., Di Rosa, F.,
678 Edgeworth, J., Shankar-Hari, M., and Hayday, A.C. (2020). A dynamic COVID-19 immune
679 signature includes associations with poor prognosis. *Nat Med* 26, 1623-1635.
- 680 Li, J., Liu, Y., and Zhang, X. (2010). Murine coronavirus induces type I interferon in
681 oligodendrocytes through recognition by RIG-I and MDA5. *J Virol* 84, 6472-6482.
- 682 Li, Y., Renner, D.M., Comar, C.E., Whelan, J.N., Reyes, H.M., Cardenas-Diaz, F.L., Truitt, R., Tan,
683 L.H., Dong, B., Alysandratos, K.D., Huang, J., Palmer, J.N., Adappa, N.D., Kohanski, M.A.,
684 Kotton, D.N., Silverman, R.H., Yang, W., Morrissey, E., Cohen, N.A., and Weiss, S.R.
685 (2020). SARS-CoV-2 induces double-stranded RNA-mediated innate immune responses
686 in respiratory epithelial derived cells and cardiomyocytes. *bioRxiv*.
- 687 Liao, M., Liu, Y., Yuan, J., Wen, Y., Xu, G., Zhao, J., Cheng, L., Li, J., Wang, X., Wang, F., Liu, L.,
688 Amit, I., Zhang, S., and Zhang, Z. (2020). Single-cell landscape of bronchoalveolar
689 immune cells in patients with COVID-19. *Nature Medicine* 26, 842-844.
- 690 Lindenbach, B.D. (2009). Measuring HCV infectivity produced in cell culture and in vivo.
691 *Methods Mol Biol* 510, 329-336.
- 692 Liu, G., Lee, J.H., Parker, Z.M., Acharya, D., Chiang, J.J., Van Gent, M., Riedl, W., Davis-Gardner,
693 M.E., Wies, E., Chiang, C., and Gack, M.U. (2020). ISG15-dependent Activation of the
694 RNA Sensor MDA5 and its Antagonism by the SARS-CoV-2 papain-like protease. *bioRxiv*.
- 695 Lucas, C., Wong, P., Klein, J., Castro, T.B.R., Silva, J., Sundaram, M., Ellingson, M.K., Mao, T., Oh,
696 J.E., Israelow, B., Takahashi, T., Tokuyama, M., Lu, P., Venkataraman, A., Park, A.,
697 Mohanty, S., Wang, H., Wyllie, A.L., Vogels, C.B.F., Earnest, R., Lapidus, S., Ott, I.M.,
698 Moore, A.J., Muenker, M.C., Fournier, J.B., Campbell, M., Odio, C.D., Casanovas-
699 Massana, A., Herbst, R., Shaw, A.C., Medzhitov, R., Schulz, W.L., Grubaugh, N.D., Dela
700 Cruz, C., Farhadian, S., Ko, A.I., Omer, S.B., and Iwasaki, A. (2020). Longitudinal analyses
701 reveal immunological misfiring in severe COVID-19. *Nature* 584, 463-469.

- 702 Mahase, E. (2020). Covid-19: Anti-TNF drug adalimumab to be trialled for patients in the
703 community. *BMJ* 371, m3847.
- 704 Mehra, M.R., Desai, S.S., Kuy, S., Henry, T.D., and Patel, A.N. (2020). Cardiovascular Disease,
705 Drug Therapy, and Mortality in Covid-19. *New England Journal of Medicine* 382, e102.
- 706 Miorin, L., Kehrer, T., Sanchez-Aparicio, M.T., Zhang, K., Cohen, P., Patel, R.S., Cupic, A., Makio,
707 T., Mei, M., Moreno, E., Danziger, O., White, K.M., Rathnasinghe, R., Uccellini, M., Gao,
708 S., Aydillo, T., Mena, I., Yin, X., Martin-Sancho, L., Krogan, N.J., Chanda, S.K., Schotsaert,
709 M., Wozniak, R.W., Ren, Y., Rosenberg, B.R., Fontoura, B.M.A., and García-Sastre, A.
710 (2020). SARS-CoV-2 Orf6 hijacks Nup98 to block STAT nuclear import and antagonize
711 interferon signaling. *Proc Natl Acad Sci U S A* 117, 28344-28354.
- 712 Nicholls, J.M., Poon, L.L., Lee, K.C., Ng, W.F., Lai, S.T., Leung, C.Y., Chu, C.M., Hui, P.K., Mak, K.L.,
713 Lim, W., Yan, K.W., Chan, K.H., Tsang, N.C., Guan, Y., Yuen, K.Y., and Peiris, J.S. (2003).
714 Lung pathology of fatal severe acute respiratory syndrome. *Lancet* 361, 1773-1778.
- 715 Ogando, N.S., Dalebout, T.J., Zevenhoven-Dobbe, J.C., Limpens, R., Van Der Meer, Y., Caly, L.,
716 Druce, J., De Vries, J.J.C., Kikkert, M., Bárcena, M., Sidorov, I., and Snijder, E.J. (2020).
717 SARS-coronavirus-2 replication in Vero E6 cells: replication kinetics, rapid adaptation
718 and cytopathology. *J Gen Virol* 101, 925-940.
- 719 Pairo-Castineira, E., Clohisey, S., Klaric, L., Bretherick, A.D., Rawlik, K., Pasko, D., Walker, S.,
720 Parkinson, N., Fourman, M.H., Russell, C.D., Furniss, J., Richmond, A., Gountouna, E.,
721 Wrobel, N., Harrison, D., Wang, B., Wu, Y., Meynert, A., Griffiths, F., Oosthuizen, W.,
722 Kousathanas, A., Moutsianas, L., Yang, Z., Zhai, R., Zheng, C., Grimes, G., Beale, R., Millar,
723 J., Shih, B., Keating, S., Zechner, M., Haley, C., Porteous, D.J., Hayward, C., Yang, J.,
724 Knight, J., Summers, C., Shankar-Hari, M., Klenerman, P., Turtle, L., Ho, A., Moore, S.C.,
725 Hinds, C., Horby, P., Nichol, A., Maslove, D., Ling, L., Mcauley, D., Montgomery, H.,
726 Walsh, T., Pereira, A., Renieri, A., Millar, J., Nichol, A., Walsh, T., Openshaw, P.J.M.,
727 Shankar-Hari, M., Ponting, C., Meikle, J., Finernan, P., Mcmaster, E., Law, A., Baillie, J.K.,
728 Paterson, T., Wackett, T., Armstrong, R., Clark, R., Coutts, A., Donnelly, L., Gilchrist, T.,
729 Hafezi, K., Macgillivray, L., Maclean, A., McCafferty, S., Morrice, K., Weaver, J., Boz, C.,
730 Golightly, A., Ward, M., Mal, H., Szoor-Mcelhinney, H., Brown, A., Hendry, R., Stenhouse,
731 A., Cullum, L., Law, D., Law, S., Law, R., Swets, M., Day, N., Taneski, F., Duncan, E.,
732 Parkinson, N., Collier, D., Wood, S., Zak, A., Borra, C., Matharu, M., May, P., Alldis, Z., et
733 al. (2020). Genetic mechanisms of critical illness in Covid-19. *Nature*.
- 734 Paranjpe, I., Russak, A.J., De Freitas, J.K., Lala, A., Miotto, R., Vaid, A., Johnson, K.W., Danieleotto,
735 M., Golden, E., Meyer, D., Singh, M., Somani, S., Kapoor, A., O'hagan, R., Manna, S.,
736 Nangia, U., Jaladanki, S.K., O'reilly, P., Huckins, L.M., Glowe, P., Kia, A., Timsina, P.,
737 Freeman, R.M., Levin, M.A., Jhang, J., Firpo, A., Kovatch, P., Finkelstein, J., Aberg, J.A.,
738 Bagiella, E., Horowitz, C.R., Murphy, B., Fayad, Z.A., Narula, J., Nestler, E.J., Fuster, V.,
739 Cordon-Cardo, C., Charney, D., Reich, D.L., Just, A., Bottinger, E.P., Charney, A.W.,
740 Glicksberg, B.S., and Nadkarni, G.N. (2020). Retrospective cohort study of clinical
741 characteristics of 2199 hospitalised patients with COVID-19 in New York City. *BMJ Open*
742 10, e040736.
- 743 Park, A., and Iwasaki, A. (2020). Type I and Type III Interferons - Induction, Signaling, Evasion,
744 and Application to Combat COVID-19. *Cell Host Microbe* 27, 870-878.

- 745 Rasaiyaah, J., Tan, C.P., Fletcher, A.J., Price, A.J., Blondeau, C., Hilditch, L., Jacques, D.A.,
746 Selwood, D.L., James, L.C., Noursadeghi, M., and Towers, G.J. (2013). HIV-1 evades
747 innate immune recognition through specific cofactor recruitment. *Nature* 503, 402-405.
- 748 Rebendenne, A., Chaves, A., Tauziet, M., Maarifi, G., Bonaventure, B., Planès, R., Mckellar, J.,
749 Nisole, S., Arnaud-Arnould, M., Moncorgé, O., and Goujon, C. (2020). SARS-CoV-2
750 replication triggers an MDA-5-dependent interferon production which is unable to
751 efficiently control replication. *bioRxiv*, 2020.2010.2028.358945.
- 752 Reed, L.J.M., H (1938). A simple method of estimating fifty percent end points. *Am. J. Hyg.* 27,
753 493-497.
- 754 Rehwinkel, J., Tan, C.P., Goubau, D., Schulz, O., Pichlmair, A., Bier, K., Robb, N., Vreede, F.,
755 Barclay, W., Fodor, E., and Reis E Sousa, C. (2010). RIG-I detects viral genomic RNA
756 during negative-strand RNA virus infection. *Cell* 140, 397-408.
- 757 Rodrigues, T.S., De Sá, K.S.G., Ishimoto, A.Y., Becerra, A., Oliveira, S., Almeida, L., Gonçalves,
758 A.V., Perucello, D.B., Andrade, W.A., Castro, R., Veras, F.P., Toller-Kawahisa, J.E.,
759 Nascimento, D.C., De Lima, M.H.F., Silva, C.M.S., Caetite, D.B., Martins, R.B., Castro, I.A.,
760 Pontelli, M.C., De Barros, F.C., Do Amaral, N.B., Giannini, M.C., Bonjorno, L.P., Lopes,
761 M.I.F., Santana, R.C., Vilar, F.C., Auxiliadora-Martins, M., Luppino-Assad, R., De Almeida,
762 S.C.L., De Oliveira, F.R., Batah, S.S., Siyuan, L., Benatti, M.N., Cunha, T.M., Alves-Filho,
763 J.C., Cunha, F.Q., Cunha, L.D., Frantz, F.G., Kohlsdorf, T., Fabro, A.T., Arruda, E., De
764 Oliveira, R.D.R., Louzada-Junior, P., and Zamboni, D.S. (2021). Inflammasomes are
765 activated in response to SARS-CoV-2 infection and are associated with COVID-19
766 severity in patients. *J Exp Med* 218.
- 767 Roth-Cross, J.K., Bender, S.J., and Weiss, S.R. (2008). Murine coronavirus mouse hepatitis virus
768 is recognized by MDA5 and induces type I interferon in brain macrophages/microglia. *J
769 Virol* 82, 9829-9838.
- 770 Schindelin, J., Arganda-Carreras, I., Frise, E., Kaynig, V., Longair, M., Pietzsch, T., Preibisch, S.,
771 Rueden, C., Saalfeld, S., Schmid, B., Tinevez, J.Y., White, D.J., Hartenstein, V., Eliceiri, K.,
772 Tomancak, P., and Cardona, A. (2012). Fiji: an open-source platform for biological-image
773 analysis. *Nat Methods* 9, 676-682.
- 774 Stanifer, M.L., Kee, C., Cortese, M., Zumaran, C.M., Triana, S., Mukenhirn, M., Kraeusslich, H.G.,
775 Alexandrov, T., Bartenschlager, R., and Boulant, S. (2020). Critical Role of Type III
776 Interferon in Controlling SARS-CoV-2 Infection in Human Intestinal Epithelial Cells. *Cell
777 Rep* 32, 107863.
- 778 Sumner, R.P., Harrison, L., Touizer, E., Peacock, T.P., Spencer, M., Zuliani-Alvarez, L., and
779 Towers, G.J. (2020). Disrupting HIV-1 capsid formation causes cGAS sensing of viral DNA.
780 *The EMBO journal* 39, e103958-e103958.
- 781 Sumner, R.P., Thorne, L.G., Fink, D.L., Khan, H., Milne, R.S., and Towers, G.J. (2017). Are
782 Evolution and the Intracellular Innate Immune System Key Determinants in HIV
783 Transmission? *Frontiers in immunology* 8, 1246-1246.
- 784 Szabo, P.A., Dogra, P., Gray, J.I., Wells, S.B., Connors, T.J., Weisberg, S.P., Krupska, I.,
785 Matsumoto, R., Poon, M.M.L., Idzikowski, E., Morris, S.E., Pasin, C., Yates, A.J., Ku, A.,
786 Chait, M., Davis-Porada, J., Zhou, J., Steinle, M., Mackay, S., Saqi, A., Baldwin, M., Sims,
787 P.A., and Farber, D.L. (2020). Analysis of respiratory and systemic immune responses in
788 COVID-19 reveals mechanisms of disease pathogenesis. *medRxiv*.

- 789 Totura, A.L., and Baric, R.S. (2012). SARS coronavirus pathogenesis: host innate immune
790 responses and viral antagonism of interferon. *Curr Opin Virol* 2, 264-275.
- 791 Treibel, T.A., Manisty, C., Burton, M., McKnight, Á., Lambourne, J., Augusto, J.B., Couto-Parada,
792 X., Cutino-Moguel, T., Noursadeghi, M., and Moon, J.C. (2020). COVID-19: PCR screening
793 of asymptomatic health-care workers at London hospital. *Lancet* 395, 1608-1610.
- 794 Wang, L.F., and Eaton, B.T. (2007). Bats, civets and the emergence of SARS. *Curr Top Microbiol*
795 *Immunol* 315, 325-344.
- 796 Williamson, E.J., Walker, A.J., Bhaskaran, K., Bacon, S., Bates, C., Morton, C.E., Curtis, H.J.,
797 Mehrkar, A., Evans, D., Inglesby, P., Cockburn, J., McDonald, H.I., Mackenna, B.,
798 Tomlinson, L., Douglas, I.J., Rentsch, C.T., Mathur, R., Wong, A.Y.S., Grieve, R., Harrison,
799 D., Forbes, H., Schultze, A., Croker, R., Parry, J., Hester, F., Harper, S., Perera, R., Evans,
800 S.J.W., Smeeth, L., and Goldacre, B. (2020). Factors associated with COVID-19-related
801 death using OpenSAFELY. *Nature* 584, 430-436.
- 802 Wolff, D., Nee, S., Hickey, N.S., and Marschollek, M. (2020). Risk factors for Covid-19 severity
803 and fatality: a structured literature review. *Infection*.
- 804 Wu, B., Peisley, A., Richards, C., Yao, H., Zeng, X., Lin, C., Chu, F., Walz, T., and Hur, S. (2013).
805 Structural basis for dsRNA recognition, filament formation, and antiviral signal activation
806 by MDA5. *Cell* 152, 276-289.
- 807 Yuen, C.K., Lam, J.Y., Wong, W.M., Mak, L.F., Wang, X., Chu, H., Cai, J.P., Jin, D.Y., To, K.K., Chan,
808 J.F., Yuen, K.Y., and Kok, K.H. (2020). SARS-CoV-2 nsp13, nsp14, nsp15 and orf6 function
809 as potent interferon antagonists. *Emerg Microbes Infect* 9, 1418-1428.
- 810 Zang, R., Gomez Castro, M.F., Mccune, B.T., Zeng, Q., Rothlauf, P.W., Sonnek, N.M., Liu, Z.,
811 Brulois, K.F., Wang, X., Greenberg, H.B., Diamond, M.S., Ciorba, M.A., Whelan, S.P.J., and
812 Ding, S. (2020). TMPRSS2 and TMPRSS4 promote SARS-CoV-2 infection of human small
813 intestinal enterocytes. *Sci Immunol* 5.
- 814 Zhang, Q., Bastard, P., Liu, Z., Le Pen, J., Moncada-Velez, M., Chen, J., Ogishi, M., Sabli, I.K.D.,
815 Hodeib, S., Korol, C., Rosain, J., Bilguvar, K., Ye, J., Bolze, A., Bigio, B., Yang, R., Arias,
816 A.A., Zhou, Q., Zhang, Y., Onodi, F., Korniotis, S., Karpf, L., Philippot, Q., Chbihi, M.,
817 Bonnet-Madin, L., Dorgham, K., Smith, N., Schneider, W.M., Razooky, B.S., Hoffmann,
818 H.H., Michailidis, E., Moens, L., Han, J.E., Lorenzo, L., Bizien, L., Meade, P., Neehus, A.L.,
819 Ugurbil, A.C., Corneau, A., Kerner, G., Zhang, P., Rapaport, F., Seeleuthner, Y., Manry, J.,
820 Masson, C., Schmitt, Y., Schlüter, A., Le Voyer, T., Khan, T., Li, J., Fellay, J., Roussel, L.,
821 Shahrooei, M., Alosaimi, M.F., Mansouri, D., Al-Saud, H., Al-Mulla, F., Almourfi, F., Al-
822 Muhsen, S.Z., Alsohime, F., Al Turki, S., Hasanato, R., Van De Beek, D., Biondi, A., Bettini,
823 L.R., D'angio, M., Bonfanti, P., Imberti, L., Sottini, A., Paghera, S., Quiros-Roldan, E.,
824 Rossi, C., Oler, A.J., Tompkins, M.F., Alba, C., Vandernoot, I., Goffard, J.C., Smits, G.,
825 Migeotte, I., Haerynck, F., Soler-Palacin, P., Martin-Nalda, A., Colobran, R., Morange,
826 P.E., Keles, S., Çölkesen, F., Ozcelik, T., Yasar, K.K., Senoglu, S., Karabela §, N., Rodríguez-
827 Gallego, C., Novelli, G., Hraiech, S., Tandjaoui-Lambotte, Y., Duval, X., Laouénan, C.,
828 Snow, A.L., Dalgard, C.L., Milner, J.D., Vinh, D.C., et al. (2020). Inborn errors of type I IFN
829 immunity in patients with life-threatening COVID-19. *Science* 370.
- 830 Zhou, F., Yu, T., Du, R., Fan, G., Liu, Y., Liu, Z., Xiang, J., Wang, Y., Song, B., Gu, X., Guan, L., Wei,
831 Y., Li, H., Wu, X., Xu, J., Tu, S., Zhang, Y., Chen, H., and Cao, B. (2020). Clinical course and

832 risk factors for mortality of adult inpatients with COVID-19 in Wuhan, China: a
833 retrospective cohort study. *Lancet* 395, 1054-1062.
834

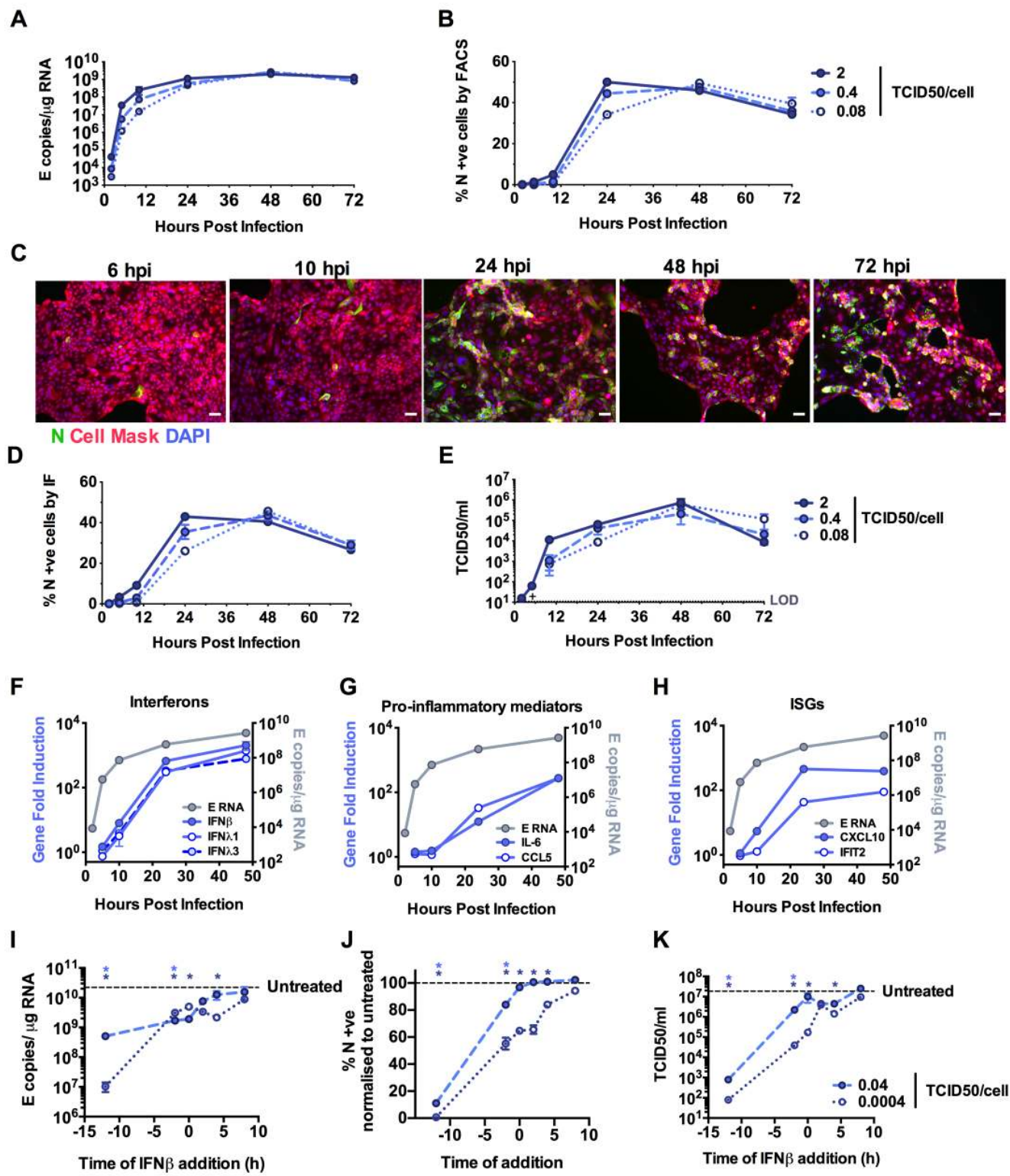


Figure 1.SARS-CoV-2 activates delayed innate immune responses in lung epithelial cells (A-H) Measurements of replication and innate immune induction in Calu-3 lung epithelial cells infected with SARS-CoV-2 at MOIs 0.08, 0.4 and 2 TCID50_{VERO}/cell. Means shown +/- SEM, n=2. (A) Replication of SARS-CoV-2 genomic and subgenomic E RNAs (qRT-PCR). (B) Quantification of N staining from cells in (A) by flow cytometry. Mean percentage of N-positive of all live-gated cells is shown +/- SEM, n=2. (C) Representative example of immunofluorescence staining of N protein (green) after SARS-CoV-2 infection of Calu-3 at MOI 0.4 TCID50_{VERO}/cell, at time points shown. Nuclei (DAPI, blue), cell mask (red). (E) Infectious virus released from cells in (A) determined by TCID50 on Vero.E6 cells, n=2. (D) Quantification of N staining in cells in (C) by immunofluorescence . (E) Infectious virus released from cells in (A) determined by TCID50 on Vero.E6 cells, n=2. (F-H) Fold induction of (F) interferons (IFNβ, IFNλ1 and IFNλ3) (G) IFN stimulated genes (CXCL10 and IFIT2) or (H) pro-inflammatory mediators (IL-6 and CCL5) each overlaid with SARS-CoV-2 E (qRT-PCR). All data from cells in (A) at MOI 0.4 TCID50_{VERO}/cell. Mean +/- SEM, n=2. (I-L) SARS-CoV-2 infection (MOIs 0.04 (closed symbols) and 0.0004 (open symbols) TCID50_{VERO}/cell) in Calu-3 cells with addition of 10ng/ml IFNβ before or after infection at time points shown, measured by (I) E RNA copies (J) N positive cells, (L) released virus (TCID50_{VERO}/cell) all measured at 24 hpi. Mean +/- SEM, n=3, One-way ANOVA Light and dark blue * indicates significance for high and low MOIs respectively.

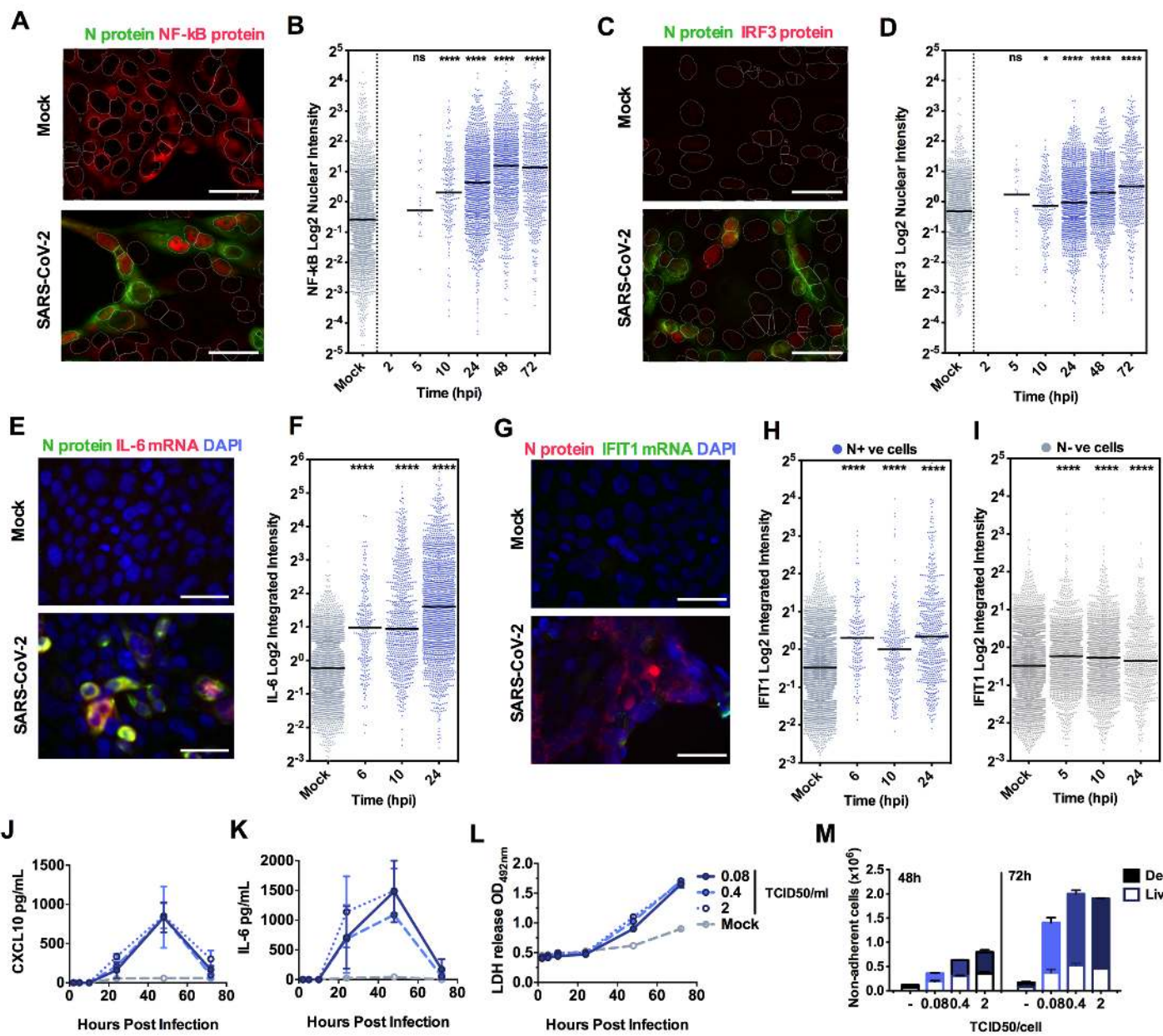


Figure 2. Peak SARS-CoV-2 replication precedes innate immune activation. (A, C) Representative images of NF-κB p65 (A) (red) and IRF3 (C) (red) nuclear localisation in mock or SARS-CoV-2 infected (MOI 0.4 TCID₅₀_{VERO}/cell) Calu-3 cells at 24 hpi. SARS-CoV-2 N protein (green), nuclei (DAPI, blue). (E and G) Representative images of IL-6 mRNA (E) detected by FISH (red) and N protein (green), or IFIT1 mRNA (G) (red) with N protein (green), both with nuclei (DAPI, blue) in mock or SARS-CoV-2 infected (MOI 0.4 TCID₅₀_{VERO}/cell) Calu-3 cells at 24 hpi. (B, D, F, H) Single cell analysis time course quantifying the Integrated Nuclear Intensity of NF-κB p65 (B), IRF3 (D), or overall integrated intensity for IL-6 (F) or IFIT1 (H) mRNA over time in N protein positive cells and N protein negative cells (E). n=2. Kruskal-Wallis test with Dunn's multiple comparison. * (p<0.05), **** (p<0.0001). (I, J) Secretion of CXCL10 (I) and IL-6 (J) by infected Calu-3 cells (MOIs 0.08, 0.4 and 2 TCID₅₀_{VERO}/cell), (ELISA). Mean +/- SEM, n=2. (K) Lactate dehydrogenase (LDH) release into culture supernatants by mock and SARS-CoV-2 infected Calu-3 cells (MOIs 0.08, 0.4 and 2 TCID₅₀_{VERO}/cell) quantified absorbance (492nm), means +/- SEM, n=2. (L) Quantification of live/dead staining of non-adherent cells recovered from supernatants of mock or SARS-CoV-2 infected Calu-3 cultures at 48 and 72 hpi. Mean +/- SEM (n=2).

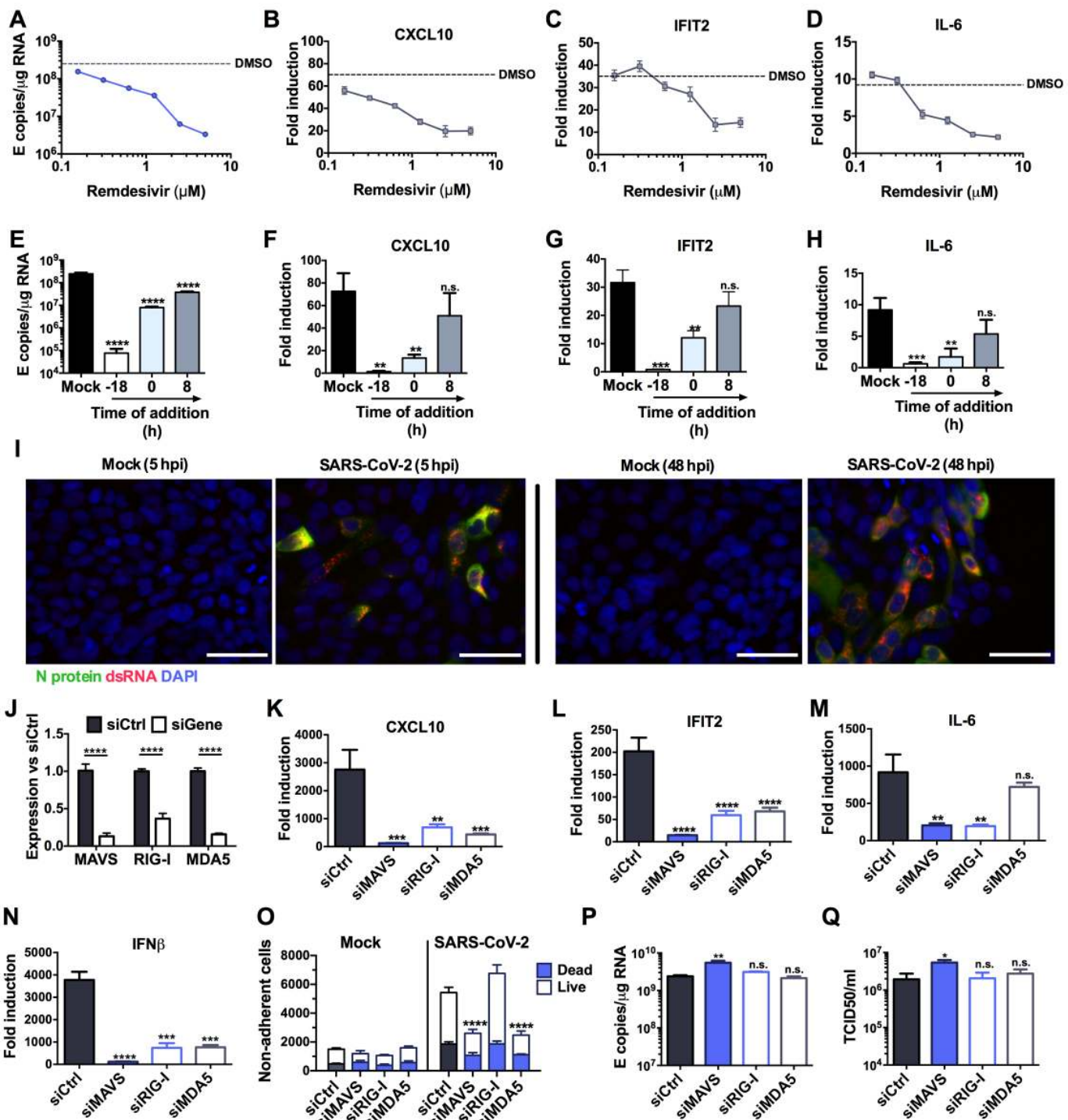


Figure 3. SARS-CoV-2 is sensed by MDA5 and RIG-I. (A-D) Measurement of (A) viral genomic and subgenomic E RNA at 24 hpi, (B) fold induction of CXCL10 from (A), (C) IFIT2 and (D) IL-6 mRNA (qRT-PCR) from (A) after Remdesivir treatment (0.125-5 μ M) of SARS-CoV-2 infected Calu-3 cells (MOI 0.04 TCID50/cell) with Remdesivir added 2h prior to infection. Mean +/- SEM, n=3. (E-H) Measurement of (E) viral genomic and subgenomic E RNA (F) fold induction of CXCL10, (G) IFIT2, (H) and IL-6 at 24 hpi, of Calu-3 cells with SARS-CoV-2 (MOI 0.04 TCID50_{VERO}/cell) with Remdesivir treatment (5 μ M) prior to, at the time of, or 8 h post-infection. Mean +/- SEM, n=3, One way ANOVA with Dunnett's multiple comparisons test to compare to untreated infected condition ('mock'), ** (p<0.01), *** (p<0.001), **** (p<0.0001). (I) Representative example of immunofluorescence staining of dsRNA (red) and N protein (green) after SARS-CoV-2 infection of Calu-3 at MOI 0.4 TCID50_{VERO}/cell, at time points shown. Nuclei (DAPI, blue). (J) RNAi mediated depletion of MAVS, RIG-I or MDA-5, reduced their expression levels as compared to siControl (siCtrl) Mean +/- SEM. Two-Way ANOVA with Sidak's multiple comparisons test, **** (p<0.0001). (K-N) Fold induction of (K) CXCL10, (L) IFIT2, (M) IL-6 or (N) IFN β in SARS-CoV-2 infected Calu-3 cells (MOI 0.04 TCID50/cell) 24 hpi. Mean +/- SEM, n=3, and compared to siCtrl for each gene by One Way ANOVA with Dunnett's multiple comparisons test, ** (p<0.01), *** (p<0.001), **** (p<0.0001), n.s. : non significant. (O) Live/dead stain counts for non-adherent cells, recovered at 48 hpi from supernatants of SARS-CoV-2 infected Calu-3 cells, depleted for MAVS, compared to siCtrl. Mean +/- SEM, n=3. Total numbers are compared to siCtrl by unpaired t-test, *** (p<0.001). Cell counts were determined by acquisition by flowcytometry for a defined period of time. Dead cells were determined by live/dead staining, means shown +/- SEM (n=3). (P-Q) (P) Viral E RNA and (Q) released infectious virus (TCID50_{VERO}/cell) at 24 hpi of infected Calu-3 cells depleted for MAVS, RIG-I or MDA5. Mean +/- SEM, n=3. Each group compared to siCtrl by One Way ANOVA with Dunnett's multiple comparisons test, * p>0.05, ** (p<0.01), n.s : non significant.

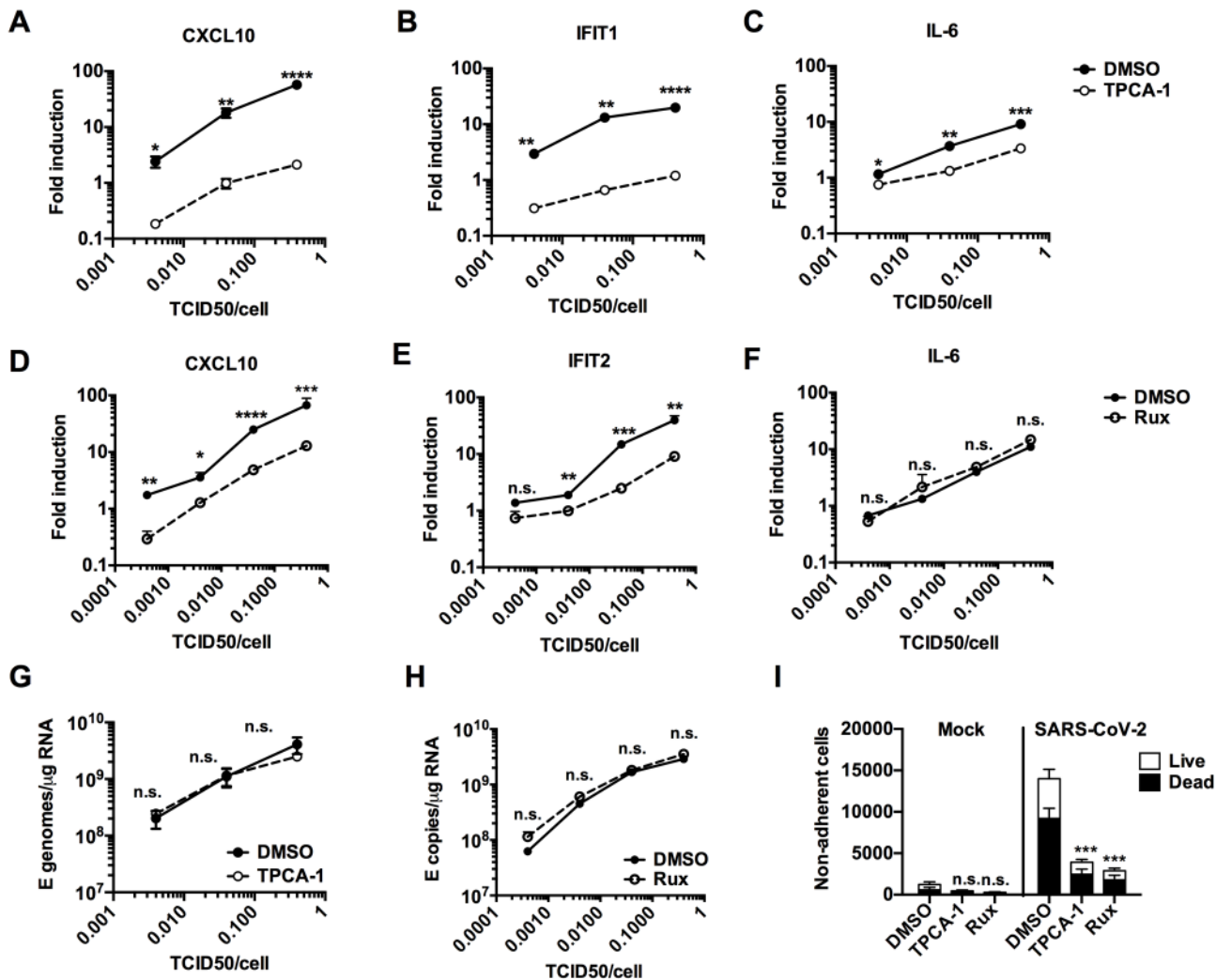


Figure 4. NF- κ B and JAK/STAT signalling drive innate immune responses. (A-C) Fold induction at 24 hpi of (A) CXCL10, (B) IFIT1 or (C) IL-6 mRNA (qRT-PCR) after Calu-3 infection with SARS-CoV-2 over a range of MOIs (0.004, 0.04, 0.4 TCID₅₀_{VERO}/cell) in the presence of 10 μ M TPCA-1 or DMSO as shown. (D-F) Fold induction at 24 hpi of (D) CXCL10, (E) IFIT2 or (F) IL-6 mRNA (RT-qPCR) after Calu-3 infection with SARS-CoV-2 over a range of MOIs (0.0004, 0.004, 0.04, 0.4 TCID₅₀_{VERO}/cell) in the presence of 2 μ M Ruxolitinib (Rux) or DMSO as shown. (G-H) Viral genomic and subgenomic E RNA at 24 hpi (RT-qPCR) with DMSO or TPCA (G) or Rux (H) treatment. (A-H) Mean +/- SEM, n=3, (A-H) Statistical comparisons are made by unpaired t test comparing inhibitor-treated to mock-treated SARS-CoV-2 infected conditions at each MOI and each timepoint. * (p<0.05), ** (p<0.01), *** (p<0.001), **** (p<0.0001). (I) Live/dead stain count from non-adherent cells recovered from supernatants of SARS-CoV-2 infected Calu-3 cultures (MOI 0.04 TCID₅₀_{VERO}/cell) 48 hpi (flow cytometry). (n=3) One Way ANOVA comparison of inhibitor-treated infected cells to mock-treated infected cells. *** (p<0.001).

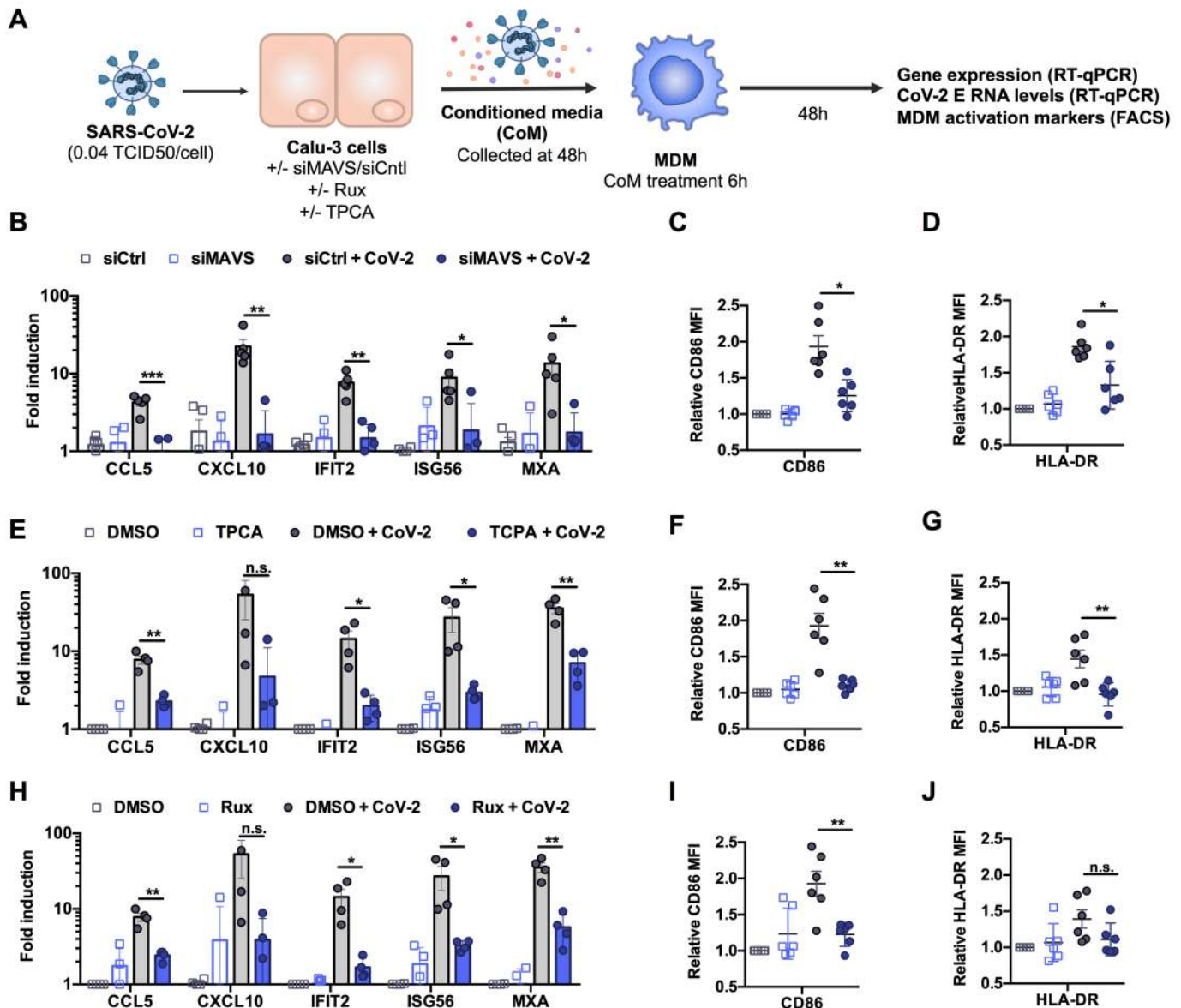


Figure 5. Epithelial responses to SARS-CoV-2 drive macrophage activation (A). Schematic of experimental design. (B-J) Calu-3 cells were transfected with siRNA targeting MAVS or non-targeting control (siCtrl) (B-D) or treated with DMSO vehicle or inhibitors 10 μ M TPCA-1 (E-G) or 2 μ M Ruxolitinib (Rux) (H-J) as shown, and were mock-infected or infected with SARS-CoV-2 at MOI 0.04 TCID₅₀_{VERO}/cell. Virus containing conditioned media (CoM) was harvested at 48 hpi. MDM were treated with Calu-3 virus containing CoM for 6 hpi, before washing and measuring MDM gene expression (B, E, H), and MDM activation markers by flowcytometry 48 h later (C,D,F,G,I,J), plotting relative median fluorescent intensity (MFI) compared to mock-infected siCtrl (C, D) or mock-infected DMSO control (F, G, I, J). Legends in (B), (E) and (H) apply to (C,D), (F,G) and (I,J) respectively. Mean +/- SEM shown, data from 4-6 independent MDM donors is shown. Statistical comparison by two-tailed paired t-test comparing MDM exposed to control infected CoM to siMAVS/inhibitor treated infected CoM. * (p<0.05), ** (p<0.01), *** (p<0.001).

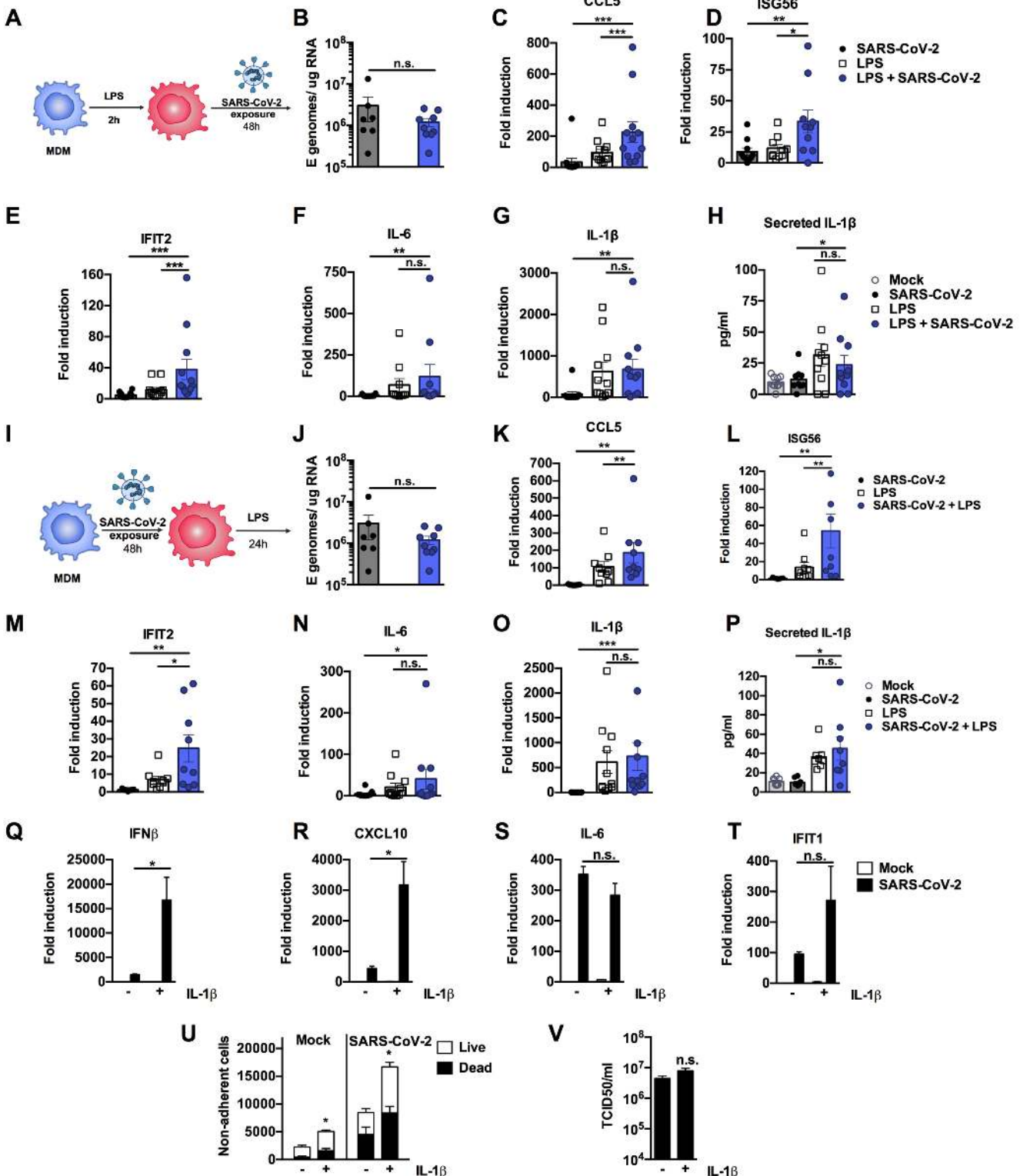


Figure 6. Pre-existing immune activation exacerbates SARS-CoV-2-dependent inflammation. (A) Schematic of experimental design. (B-H) MDM were primed with 100ng/ml LPS for 2h before exposure to SARS-CoV-2 (MOI 0.02 TCID50_{VERO}/cell). (B) Expression of genomic and subgenomic viral E RNA at 48 h post exposure in indicated conditions. (C-G) Host gene expression of (C) CCL5, (D) ISG56, (E) IFIT2, (F) IL-6 or (G) IL-1β was measured 48hpi. (H) IL-1β secretion was detected in culture supernatants at 48 hpi by ELISA. (I) Schematic of experimental design. MDM were exposed to SARS-CoV-2 (MOI 0.02 TCID50_{VERO}/cell) for 48 h and subsequently stimulated with 100ng/ml LPS for 24 h. (J) Expression of genomic and subgenomic viral E RNA 72 h post-exposure in indicated conditions. (K-L) Host gene expression of (K) CCL5, (L) ISG56, IFIT2 (M), (N) IL-6 and (O) IL-1β. (P) IL-1β secretion was detected in culture supernatants at 48 hpi by ELISA. Gene expression is shown as fold induction over untreated controls. Data from 8-13 independent donors is shown. Groups were compared as indicated by Wilcoxon matched-pairs signed rank test, *, p<0.05, ** (p<0.01), *** (p<0.001). (Q-V) Calu-3 cells were infected with SARS-CoV-2 (MOI 0.04 TCID50_{VERO}/cell) in the presence or absence of 10ng/ml IL-1β. (Q-T) Gene expression of (Q) IFNβ (R), CXCL10, (S) IL-6 and (T) IFIT1 was measured after 24h. Fold induction over untreated mock infection is shown, n=3. (U) Non-adherent cells were collected at 48h post infection and live/dead stained. Cells were acquired by flowcytometry and cell counts determined by time-gating. For statistical comparison, total cell numbers were compared. (V) Viral release into culture supernatants at 24 h was measured by TCID50 on VeroE6 cells. (Q-V) Mock and SARS-CoV-2 infected conditions were compared with or without IL1β-treatment, respectively, by unpaired T test (n=3). *, p<0.05; n.s., non-significant. Mean +/- SEM shown.